Geol. Mag. **139** (6), 2002, pp. 621–640. © 2002 Cambridge University Press
DOI: 10.1017/S0016756802006829 *Printed in the United Kingdom*

Mesozoic volcanism in the Middle East: geochemical, isotopic and petrogenetic evolution of extension-related alkali basalts from central Lebanon

ABDEL-FATTAH M. ABDEL-RAHMAN*

Department of Geology, American University of Beirut, Beirut, P.O. Box 11-0236, Lebanon

(*Received* 25 July 2001; *revised version received* 27 June 2002; *accepted* 27 June 2002)

Abstract – Mesozoic picritic and alkali basalts from central Lebanon represent a significant part of an extension-related Upper Jurassic to Upper Cretaceous discontinuous volcanic belt which occurs throughout the Middle East. Volcanism was associated with an episode of intraplate extension that followed a period of continental break-up, where Mesozoic micro-continental blocks separated from Gondwana as the Neotethys ocean opened in Jurassic times. This volcanic episode produced mafic lava flows ranging in thickness from 5 to 20 m, along with some minor pyroclastic flows. These flows are stratigraphically intercalated with thick carbonate platform deposits. The basalts are made up of about 15–20% olivine ($Fo_{78–91}$), 30–35% clinopyroxene (salite), 40–50% plagioclase ($An_{56–71}$) and opaque Fe–Ti oxides (~5%). Geochemically, the rocks exhibit a relatively wide range of SiO_2 (40.4 to 50.5 wt%) and MgO (5.1 to 15.5 wt%) contents, are relatively enriched in TiO_2 (1.7 to 3.7 wt%) and vary in composition from alkali picrite and basanite to alkali basalt. The Mg numbers range from 0.56 to 0.70, with an average of 0.63. The rocks are enriched in incompatible trace elements such as Zr (86–247 ppm), Nb (16–66 ppm) and Y (19–30 ppm). Such compositions are typical of those of HIMU-OIB and plume-related magmas. The REE patterns are fractionated ($(La/Yb)_N$ = 11), LREE enriched, and are generally parallel to subparallel. Elemental ratios such as K/P (1.1–4.7), La/Ta (11–13), La/Nb (0.57–0.70), Nb/Y (0.68–1.55) and Th/Nb (0.20–0.36) suggest that crustal contamination was minor or absent. This may be related to a rapid ascent of the magma, in agreement with the nature (mafic, oceanic-like) and the small thickness (about 12 km) of the Mesozoic crust of the Eastern Mediterranean region. The $^{143}Nd/^{144}Nd$ isotopic compositions of the lavas range from 0.512826 to 0.512886, and $^{87}Sr/^{86}Sr$ from 0.702971 to 0.703669, suggesting a HIMU-like mantle source. Trace element compositions indicate a melt segregation depth of 100–110 km, well within the garnet lherzolite stability field. The geochemical characteristics of the rocks are typical of within-plate alkali basalts, and suggest that the magmas were derived from a fertile, possibly plume-related, enriched mantle source. Petrogenetic modelling indicates that the magmas were produced by very small degrees of batch partial melting (F = 1.5%) of a primitive garnet-bearing mantle source (garnet lherzolite).

Keywords: Lebanon, alkali basalts, petrogenesis, Sr/Nd, geochemistry, mantle plumes.

1. Introduction

The products of a major extension-related volcanic episode, thought to be associated with, and following the development of, a Mesozoic passive continental margin as the Neotethys ocean opened, have been identified at several localities within the Middle East. The opening of Neotethys occurred along the north-eastern edge of Gondwana as Mesozoic micro-continental blocks (present-day southern Turkey, Greece and Cyprus) moved northwards (e.g. Garfunkel, 1989; Robertson *et al.* 1991; Laws & Wilson, 1997). Picritic to alkali basalts extending from Egypt, Palestine, Israel, to Jordan, Lebanon and Syria (Fig. 1) occur near the rifted boundary, and the transform faulted boundary between the Arabian Plate and both the African Plate and the Levantine sub-plate (Fig. 2a), respectively. Based on a large number of radiometric age determinations, the age of Mesozoic volcanism in the Middle East appears to have extended from Late Jurassic to Mid-Cretaceous times (148–90 Ma: K–Ar age; Raad, 1979; Lang & Steinitz, 1989; Shimron & Lang, 1989; Mouty *et al.* 1992; Laws & Wilson, 1997).

Several studies have been carried out on the Mesozoic basaltic rocks of Israel (e.g. Shimron & Lang, 1989; Garfunkel, 1992; Kohn, Lang & Steinitz, 1993; Gvirtzman, Garfunkel & Rotstein, 1994; Laws & Wilson, 1997). However, those cropping out in Lebanon and Syria have been little investigated. Renouard (1951), Dubertret (1955, 1963, 1975), Arkel (1956) and Al-Nadi (I. Al-Nadi, unpub. M.Sc. thesis, American Univ. of Beirut, Lebanon, 1966) described the field relations of the Lebanese Mesozoic alkali basalts indicating that they form flows, bedded tuffs and agglomerates, which were emplaced mostly in a subaerial environment. The petrography of these

* E-mail: arahman@aub.edu.lb

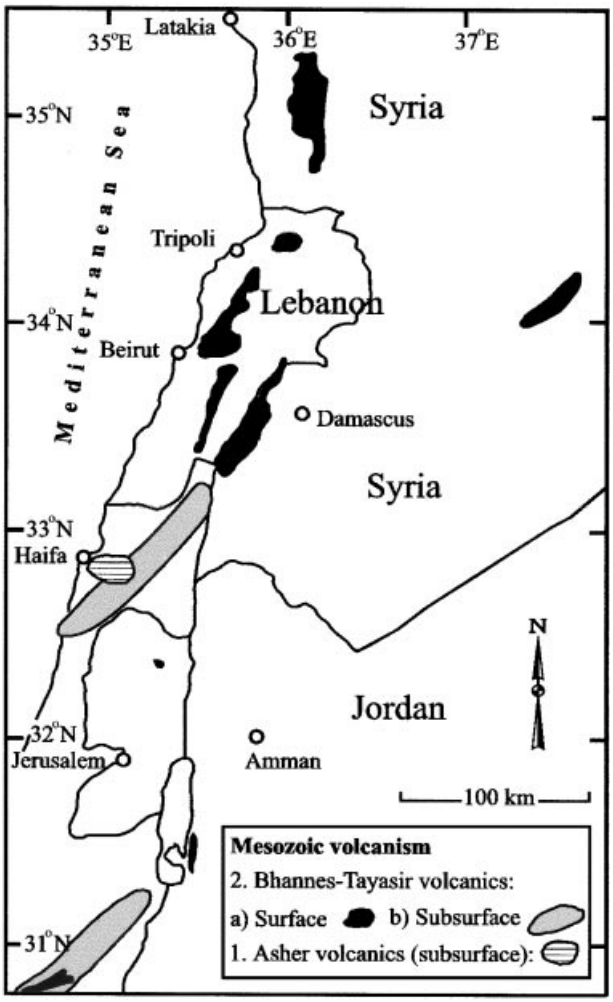

Figure 1. Regional geological map showing the distribution of Mesozoic basalts in the Middle East (modified from Laws & Wilson, 1997).

rocks was described by Kuttayneh (S. Kuttayneh, unpub. M.Sc. thesis, American Univ. of Beirut, Lebanon, 1967). Raad (1979) used the K–Ar method to date some of these basaltic rocks; he obtained an age of 118 ± 6 Ma. He also provided partial major element analyses for a few samples. More recently, Laws & Wilson (1997) did a regional general study on the tectonism and associated magmatism in the Middle East; they considered the basaltic magmas of this region to have been extension-related, derived from an enriched mantle source, and that magma ascent was facilitated by large-scale faults.

The aim of this contribution is to present a detailed mineralogical, chemical and isotopic study on the Lebanese Mesozoic alkali basalts, to evaluate their source characteristics and magma evolution, and to assess the possible link between magmatism and mantle plumes. In this study, the volcanism will be evaluated in the context of Mesozoic continental breakup, the Tethyan geodynamic evolution, and the nature of the Levantine (Eastern Mediterranean) crust.

2. The geological context

Mesozoic volcanism in the Middle East may have occurred in association with an episode of extension-induced fractures which represented precursors to the rifted plate margins between the Arabian Plate and both the African Plate and the Levantine sub-plate, long before the opening of the Red Sea–Dead Sea rift systems. The Mesozoic alkali basaltic province of the Middle East consists of discontinuous exposures occurring along an approximately 600 km long belt in the Eastern Mediterranean region (Fig. 1). The basaltic rocks of the Lebanese crust are the largest and best-preserved part of this volcanic belt. The basaltic formation is exposed in central Lebanon (Fig. 2) in the form of a series of flows occurring within a 3.5 km thick Mesozoic carbonate sequence (Dubertret, 1955; Abdel-Rahman & Nader, 2002). This sequence is part of a much larger carbonate platform deposited mostly during the Jurassic–Cretaceous period, at the northwestern margin of the Arabian Plate, covering a large part of the Eastern Mediterranean region.

The Lebanese crust is cross-cut by a major NE–SW-trending fault (the Yammouneh Fault) which represents a transform plate boundary (Fig. 2a,c) between the Arabian Plate and the Levantine sub-plate. This fault links the Dead Sea transform (further to the south), and its northern extension (the Ghab Fault of Syria) which apparently joins the continental collision zone at the left-lateral East Anatolian Fault of southeastern Turkey (Fig. 2a). This more recent transform fault system shows 100–105 km of left-lateral Neogene motion (Garfunkel, 1981); it was probably inactive during the eruption of the Mesozoic basalts.

The Mesozoic basalts of Lebanon represent the main component of an Upper Jurassic formation known locally as the 'Bhannes' Formation. The 'Bhannes' Formation (50–150 m thick) consists mainly of basaltic eruptive rocks and minor carbonate rocks. The eruptive rocks occur in the form of minor sills, subaerial lava flows and associated pyroclastic rocks (5–20 m thick), intercalating with marine sediments (limestone and marl beds) of variable thickness (1–15 m thick) formed during periods of transgression. Such periods of transgression have alternated with periods of regression, during which eruptions of these volcanic materials occurred. The lava flows are occasionally columnar jointed and commonly show spheroidal weathering, but appear to lack pillow lava structures. The basaltic rocks exhibit variable degrees of vesicularity. These rocks are non-metamorphosed, generally fresh, but in some outcrops the rocks are moderately altered. The pyroclastic rocks are made up of tuffs, lapilli and blocks of basalt. The K–Ar age of the investigated Mesozoic basaltic rocks of Central Lebanon, as determined by Raad (1979), is 118 ± 6 Ma. The 'Bhannes' Formation overlies the Middle Jurassic 'Kesrouane' Formation, consisting of a thick (1.0–1.7 km) sequence of shallow, inner to

https://doi.org/10.1017/S0016756802006829 Published online by Cambridge University Press

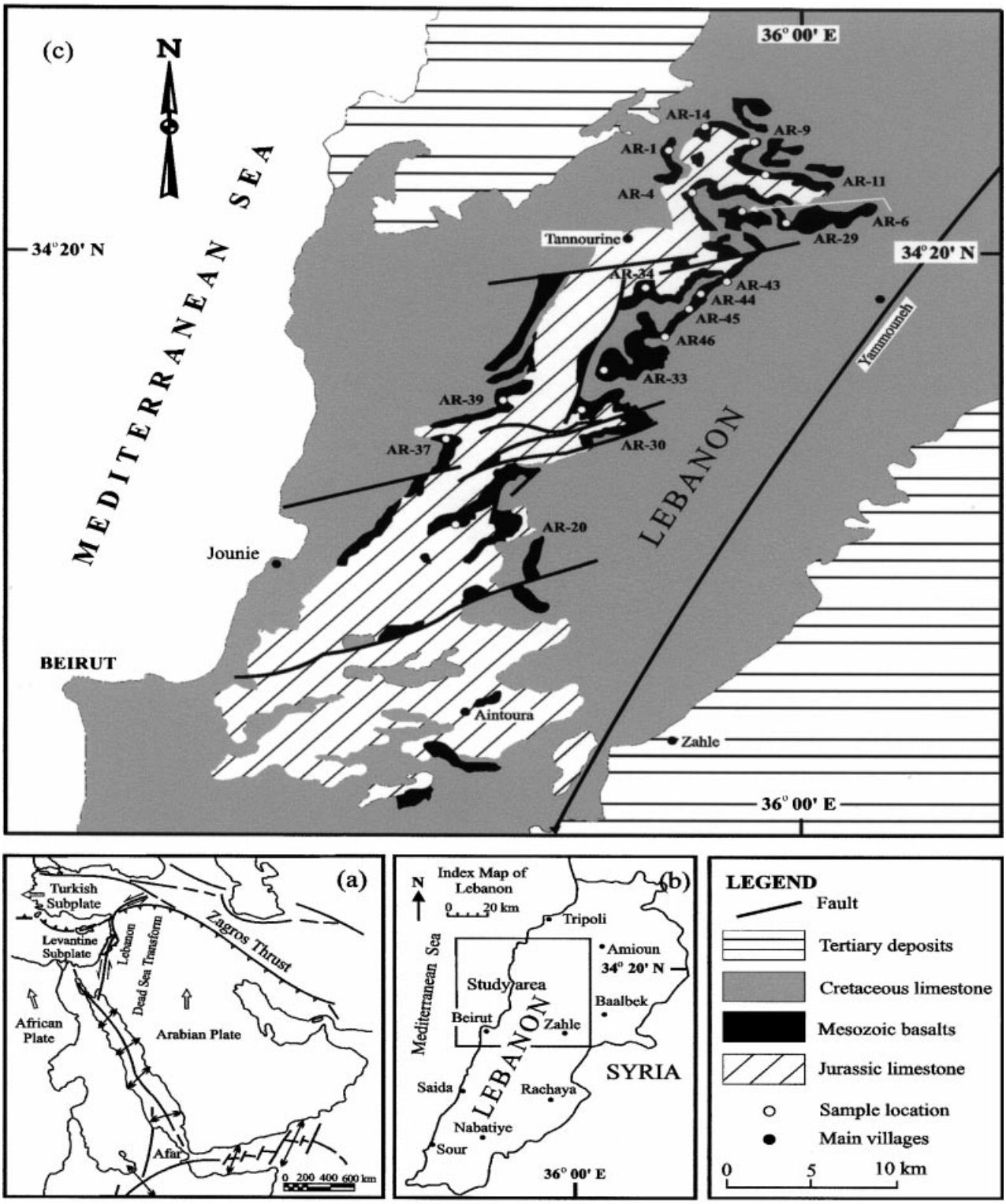

Figure 2. Simplified geological map of central Lebanon (map c; after Dubertret, 1955) showing the distribution of the Mesozoic basaltic rocks which occur within a thick sequence of sedimentary carbonate formations; locations of the basaltic samples analysed in this study are shown. Diagram (a) is a map showing the main structural-tectonic elements in the region, and (b) is a location map for the area of study.

middle shelf, massive dolomite and limestone rocks (Dubertret, 1955, 1963; Walley, 1997), and is overlain by carbonate (micritic limestone) rocks of the 'Bikfaya' Formation.

Two phases of Mesozoic volcanism have been identified in Israel: a Late Triassic–Early Jurassic phase that produced basaltic rocks known as the 'Asher Volcanics' and a Late Jurassic–Early Cretaceous phase that produced the 'Tayasir Volcanics'. As described in Dvorkin & Kohn (1989) and Garfunkel (1989), the

https://doi.org/10.1017/S0016756802006829 Published online by Cambridge University Press

'Asher' volcanic rocks are not exposed at the surface, but were encountered (at the subsurface) in the Atlit 1 and other boreholes in northern Israel (Fig. 1) unconformably overlying Late Triassic carbonate successions. The 'Asher' volcanic rocks consist of spilitized basalts, but with the uppermost zone containing relatively fresh alkali olivine basalts. These basaltic rocks range in age from 205 to 190 Ma (K–Ar ages: Lang & Steinitz, 1987). The 'Saharonim basalt' of the Makhtesh Ramon area of southern Israel was dated by Baer *et al.* (1995) at 202 to 210 Ma (K–Ar method) and was considered to belong to the 'Asher' volcanic event. The Late Jurassic–Early Cretaceous 'Tayasir' volcanic rocks are known from outcrops and from the subsurface (Fig. 1), occurring in the Negev and in the Samaria–Galilee fields in Central Israel; they range in composition from olivine basalt and trachy-basalt to trachyte (Garfunkel, 1989). Using K–Ar and Rb–Sr methods, Lang & Steinitz (1987) and Lang *et al.* (1988) produced ages ranging from 145 to 115 Ma for rocks of the 'Tayasir' magmatic event. Gvirtzman *et al.* (1996) produced an Ar–Ar age of 118 ± 1.5 Ma for basaltic ('Tayasir') rocks from the Negev field. Note that this age is identical to that produced by Raad (1979) for basalts of the 'Bhannes' Formation in central Lebanon, which is the subject of this investigation.

3. Analytical procedures

3.a. Mineral chemistry data

Mineral analyses (on olivine, pyroxene and plagioclase, as well as opaque and alteration phases) were conducted using a CAMECA Camebax (model MBI) electron microprobe at McGill University. Counts were obtained simultaneously from four wavelength-dispersion X-ray spectrometers, with a 15 KeV accelerating voltage, a 5 μm beam, and a beam current of 20 nA. Repeated analyses of analytical standards were made to ensure statistical accuracy. On-board software provided by Cameca was used in the ZAF corrections and reduction of data. The detection limit for the elements analysed is 0.2 wt %.

3.b. Whole-rock chemical data

3.b.1. Major elements

Concentrations of the major elements were determined on fused lithium-metaborate discs by X-ray fluorescence spectrometry (Philips PW 1400 Spectrometer at McGill University) using a Rh tube operated at 40 kV and 70 mA. Loss on ignition (LOI) was determined by heating powdered samples for 50 minutes at 1000 °C.

3.b.2. Trace elements

Concentrations of Ni, Cr, Sc, V and Ba were also determined on fused discs along with the major elements as described above. Concentrations of Rb, Sr, Zr, Y, Nb, Ga, Pb, U and Th were determined on pressed pellets by X-ray fluorescence (operating conditions: Rh radiation, 70 kV, 40 mA). The analytical precision, as calculated from 20 replicate analyses of one sample, is better than 1 % for most major elements and better than 5 % for most trace elements.

3.b.3. Rare earths, hafnium and tantalum

Concentrations of fourteen rare earth elements (REE; La to Lu, all except Pm) as well as Hf and Ta were determined by ICP-MS at the Memorial University of Newfoundland. A pure quartz reagent blank and several certified geological reference standards, as well as internal laboratory standards were analysed with these samples. Full details of the procedure are given in Longerich *et al.* (1990). Detection limits and reagent blanks are generally about 10 % of chondrite values. The primitive mantle values used for normalization are those of Sun & McDonough (1989).

3.c. Isotope data

Sm–Nd isotopic analyses were performed at the GEOTOP Laboratory of the Université du Québec at Montreal. Between 100 and 150 mg of powder was weighed in a high-pressure teflon vessel and mixed with a ^{149}Sm–^{150}Nd spike and HF–HNO_3 acids. The mixture was dissolved under pressure at 150 °C for one week. The resulting solution was passed through a cationic exchange resin from which the rare earth elements (REE) were recovered. Sm and Nd were subsequently separated from the other REE using a teflon powder coated with bis-2-orthophosphate acid (HDEHP) following the procedure of Richard, Shimizu & Allègre (1976). The isotopic ratios were measured on a VG Sector-54 mass spectrometer in double-filament mode with Sm and Nd samples loaded on a Ta side filament with a central Re filament. During the course of this study, the La Jolla Nd standard gave $^{143}Nd/^{144}Nd = 0.511848 \pm 16$ (2σ on 34 analyses). The precision on the concentrations and the $^{147}Sm/^{144}Nd$ ratio is better than 1 %, and total blanks for Nd or Sm were < 50 pg. For the Sr isotope analysis, the sample powders were leached in 6M HCl for several hours before commencing the chemical procedures. Sr isotope ratios were measured on the same mass spectrometer described above. Errors for the $^{87}Sr/^{86}Sr$ isotopic ratios are 2σ mean on in-run statistics and correspond to least significant digits; repeat analyses of the NBS SRM 987 gave results of 0.710241 ± 15.

4. Petrography and mineral chemistry

The rocks investigated consist essentially of plagioclase, clinopyroxene, olivine and some minor opaque

https://doi.org/10.1017/S0016756802006829 Published online by Cambridge University Press

oxides. Textures in these rocks vary from porphyritic, glomeroporphyritic and rarely aphyric, to intersertal and pilotaxitic. Olivine forms 15 to 20 vol.% of the rocks, and commonly forms euhedral to subhedral phenocrysts (1.0–2.1 mm across) set in a microcrystalline to cryptocrystalline intersertal groundmass. The latter consists of plagioclase, clinopyroxene and olivine. In most samples, olivine is generally fresh, but in some rocks it is partially altered to orange-red iddingsite and a mixture of serpentine + chlorite. Olivine phenocrysts are occasionally embayed by groundmass material, lack reaction rims involving pyroxene, and commonly form glomeroporphyritic textures with other olivine or clinopyroxene grains.

Clinopyroxene is also abundant as a phenocryst phase, and is common in the groundmass. It is typically neutral to pale beige in colour, constitutes about 30–35 vol.% of the rocks, and is rarely zoned. Plagioclase (40–50 vol.% of the rocks) forms rare phenocrysts but is a major component of the groundmass, forming tiny laths or microlites. Opaque oxides form about 5 vol.% of the rocks, occurring both as microphenocrysts and in the groundmass.

The chemical compositions of the various mineral phases are given in Table 1. The analyses are done mostly for phenocrysts. Compositional variation in clinopyroxene (Fig. 3a) is such that the Mg number ($Mg/(Mg + Fe^{2+})$) ranges from 0.73 to 0.84, and CaO ranges from 20.9 to 22.1 wt% (Table 1). Thus, the mineral is salite in composition. It is relatively enriched both in Ti and Al (0.9–3.5 wt% TiO_2 and 3.9–10.1 wt% Al_2O_3; Table 1). This is typical of clinopyroxene of alkalic lavas (e.g. Dobosi, 1989).

Olivine ranges in composition from Fo_{78} to Fo_{91}; MnO values vary from 0.15 to 0.25 wt%, and CaO contents range from 0.02 to 0.23 wt% (Table 1, Fig. 3a). Plagioclase varies in composition from An_{56} to An_{71} (Fig. 3b) and contains a very small K-component (0.01 to 0.16 ions per formula unit). The FeO content of the plagioclase is somewhat high (0.38 to 0.83 wt%). Chemical data on the opaque phases (Table 1) indicate that these are ilmenite and titaniferous magnetite.

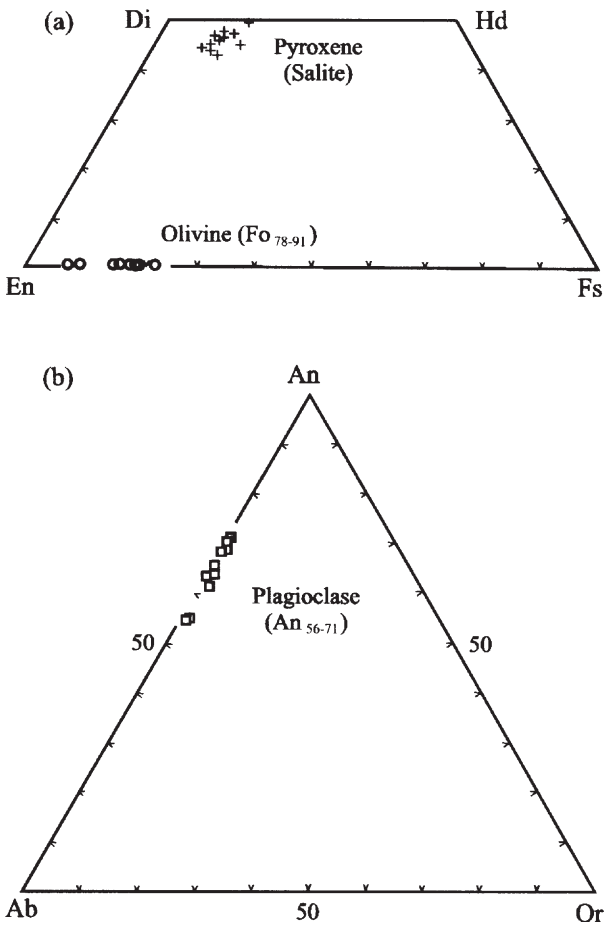

Figure 3. Pyroxene, olivine and plagioclase compositional variations in the Lebanese Mesozoic alkali basalts.

5. Geochemistry

5.a. Major and trace element geochemistry

Major and trace element data for 17 representative samples of the Lebanese Mesozoic alkali basalts are given in Table 2. Major element compositional ranges are: 40.4–50.5 wt% SiO_2, 10.4–15.3 wt% Al_2O_3, 8.4–15.4 wt% Fe_2O_3 (as total iron), 5.1–15.5 wt% MgO, 3.0–11.7 wt% CaO and 1.7–3.7 wt% TiO_2 (Table 2). Figure 4a shows that the investigated rocks can be classified as picrite, basanite, basalt and alkali basalt (Le Bas *et al.* 1986; Le Bas & Streckeisen, 1991). The Mg numbers (= molar $Mg/(Mg+Fe^{2+})$, assuming a Fe^{3+}/Fe^{2+} ratio of 0.15), range from 0.56 to 0.70 (with an average of 0.63). Such values indicate that the rocks are not primary liquids, and may have undergone some degree of olivine and clinopyroxene fractionation. The fractionation of these mafic phases is also reflected in the sharp decrease in the Ni content with decreasing Mg (from 568 ppm at 15.5 wt% MgO and 40.4 wt% SiO_2, to 130 ppm at 5.1 wt% MgO and 50.5 wt% SiO_2). Figure 5 shows that Al_2O_3 remains relatively constant; this suggests that Al was controlled by both clinopyroxene and plagioclase, as the latter continued to form up to late stages of crystallization. The rocks also exhibit a wide compositional range in Cr (151–447 ppm), V (158–276 ppm), Sr (94–967 ppm), Ba (197–861 ppm) and Rb (2–37 ppm). The rocks are generally enriched in the HFS elements such as Zr (86–247 ppm), Y (19–30 ppm) and Nb (16–66 ppm; Table 2), with ranges similar to those of OIB-type alkali basalts. For example, the OIB average composition in Nb, Y and Pb (48, 29 and 3.2 ppm, respectively; Sun & McDonough, 1989), are similar to those of the Lebanese rocks (with averages of 33, 26 and 3.9 ppm, respectively). The alkaline nature of these rocks is indicated in the (Nb/Y)–(Zr/Ti) diagram (Fig. 4b), as all data points plot exclusively in the field of alkali basalt. More specifically, the rocks exhibit elemental

https://doi.org/10.1017/S0016756802006829 Published online by Cambridge University Press

Table 1. Results of electron microprobe analysis and number of cations per formula unit of representative olivine (formulae based on 4O), pyroxene (6O), plagioclase (8O), ilmenite (3O), titaniferous magnetite (4O), and iddingsite from the Mesozoic basalts of Lebanon

	AR-1	AR-9	AR-14	AR-43	AR-45	AR-1	AR-6	AR-29	AR-43	AR-45	AR-6	AR-14	AR-20	AR-43	AR-45	AR-43	AR-45	AR-14	AR-6	AR-37	AR-45
Sample			Olivine					Pyroxene					Plagioclase			Ilmenite		Ti-magnetite		Iddingsite	
SiO_2	38.90	39.57	39.26	40.74	38.30	44.34	46.95	47.72	50.78	47.43	53.33	52.13	52.55	51.41	52.64	0.04	0.02	1.76	0.36	31.54	31.52
TiO_2	0.02	0.00	0.00	0.00	0.01	3.47	2.71	2.58	0.87	2.07	0.13	0.12	0.04	0.08	0.16	48.84	51.18	25.33	22.20	0.17	0.24
Al_2O_3	0.06	0.07	0.07	0.01	0.04	10.07	6.42	6.04	3.89	6.08	28.30	30.01	29.91	30.34	29.73	0.13	0.10	3.03	1.78	10.47	10.48
FeO	20.25	14.93	15.71	10.48	17.02	7.50	8.41	7.44	5.47	6.73	0.83	0.61	0.38	0.53	0.80	46.07	44.29	63.91	72.07	31.00	31.52
MnO	0.25	0.18	0.18	0.15	0.21	0.14	0.16	0.11	0.12	0.11	0.00	0.00	0.00	0.00	0.00	0.51	0.50	1.49	3.01	0.16	0.15
MgO	41.12	44.99	44.54	49.05	43.50	11.45	13.28	13.39	15.95	14.31	0.03	0.07	0.20	0.15	0.02	3.41	3.50	2.17	0.09	15.37	15.60
CaO	0.23	0.22	0.19	0.02	0.23	21.26	20.92	22.00	21.32	22.10	11.57	13.20	13.34	13.89	12.73	0.07	0.05	0.92	0.05	0.74	0.67
Na_2O	0.02	0.02	0.00	0.00	0.00	0.64	0.46	0.49	0.40	0.40	4.88	4.06	3.89	3.63	4.18	-	-	-	-	0.32	0.21
K_2O	0.00	0.00	0.00	0.00	0.01	0.00	0.00	0.01	0.00	0.02	0.32	0.25	0.14	0.16	0.27	-	-	-	-	0.45	0.52
Cr_2O_3	0.00	0.02	0.01	0.00	0.00	0.22	0.09	0.20	0.82	0.62	-	-	-	-	-	0.07	0.05	0.44	0.13	0.22	0.23
NiO	0.05	0.18	0.17	0.31	0.02	0.00	0.00	0.00	0.00	0.02	-	-	-	-	-	-	-	-	-	-	-
Total	100.90	100.18	100.13	100.76	99.34	99.09	99.40	99.98	99.62	99.89	99.39	100.45	100.45	100.19	100.53	99.14	99.69	99.05	99.69	90.44	91.14
Si	0.993	0.993	0.990	0.995	0.981	1.675	1.769	1.783	1.876	1.772	2.439	2.365	2.378	2.340	2.384	0.001	0.001	0.066	0.014		
Ti	0.000	0.000	0.000	0.000	0.000	0.099	0.077	0.073	0.024	0.058	0.004	0.004	0.001	0.003	0.005	0.936	0.962	0.716	0.665		
Al	0.002	0.002	0.002	0.000	0.001	0.448	0.285	0.266	0.169	0.268	1.525	1.605	1.595	1.628	1.587	0.000	0.003	0.134	0.084		
Fe	0.000	0.313	0.331	0.214	0.364	0.237	0.265	0.233	0.169	0.210	0.032	0.023	0.014	0.020	0.030	0.982	0.926	2.009	2.401		
Mn	0.005	0.004	0.004	0.003	0.005	0.004	0.005	0.003	0.004	0.003	0.000	0.000	0.000	0.000	0.000	0.011	0.011	0.047	0.102		
Mg	1.565	1.683	1.674	1.786	1.660	0.645	0.746	0.746	0.878	0.797	0.002	0.005	0.013	0.010	0.001	0.130	0.130	0.122	0.005		
Ca	0.006	0.007	0.005	0.001	0.006	0.861	0.844	0.881	0.844	0.885	0.567	0.642	0.647	0.677	0.618	0.002	0.001	0.037	0.002		
Na	0.001	0.000	0.000	0.000	0.000	0.047	0.034	0.036	0.029	0.029	0.433	0.357	0.341	0.320	0.367	-	-	-	-		
K	0.000	0.000	0.000	0.000	0.000	0.000	0.000	0.000	0.000	0.001	0.019	0.014	0.008	0.009	0.160	-	-	-	-		
Cr	0.000	0.000	0.000	0.000	0.000	0.007	0.003	0.006	0.024	0.018	-	-	-	-	-	0.001	0.001	0.013	0.004		
Ni	0.001	0.004	0.003	0.006	0.000	0.000	0.000	0.000	0.000	0.001	-	-	-	-	-	-	-	-	-		
Sum	3.006	3.006	3.009	3.005	3.019	4.022	4.027	4.026	4.017	4.042	5.020	5.015	4.998	5.008	5.008	2.062	2.035	3.144	3.277		

Table 2. Major and trace element composition (in wt %, and ppm, respectively) of representative samples of the Mesozoic basalts of Lebanon

Sample	AR-1	AR-4	AR-6	AR-9	AR-11	AR-14	AR-20	AR-29	AR-30	AR-33	AR-34	AR-37	AR-39	AR-43	AR-44	AR-45	AR-46	Average
SiO_2	43.44	43.79	47.10	41.59	46.39	43.63	46.96	44.03	43.20	40.37	43.84	50.45	44.17	47.41	46.51	44.90	45.02	44.87
TiO_2	2.70	2.56	2.44	3.69	2.51	2.52	1.77	2.43	2.52	1.67	2.42	1.88	2.40	2.36	2.14	2.33	2.34	2.39
Al_2O_3	14.33	13.66	14.60	14.43	13.89	13.94	14.33	13.34	13.41	10.38	12.75	15.28	12.83	14.50	13.78	13.72	13.08	13.66
Fe_2O_3*	11.94	13.79	10.76	14.00	11.83	13.84	11.08	11.68	14.36	15.44	12.92	8.37	12.59	10.87	10.64	10.53	12.49	12.18
MgO	7.11	9.72	6.78	7.49	8.68	9.20	8.09	10.30	9.90	15.50	10.95	5.05	10.41	7.27	8.67	7.21	9.47	8.93
MnO	0.22	0.19	0.24	0.19	0.16	0.20	0.08	0.19	0.18	0.17	0.19	0.08	0.17	0.20	0.17	0.21	0.18	0.18
CaO	10.37	9.32	9.70	9.70	9.80	9.93	8.44	10.60	8.93	4.90	10.52	2.96	10.62	9.96	8.41	11.66	10.79	9.21
Na_2O	1.82	2.97	2.92	4.39	2.83	3.14	2.51	1.79	2.80	1.83	2.33	8.69	1.63	2.78	2.26	2.45	2.57	2.47
K_2O	1.20	1.18	0.83	0.67	0.89	1.14	0.18	0.21	0.98	0.44	1.04	0.95	1.07	0.78	0.86	0.72	0.87	1.28
P_2O_5	0.62	0.59	0.35	0.74	0.40	0.53	0.23	0.36	0.58	0.36	0.45	0.24	0.44	0.32	0.28	0.31	0.35	0.42
LOI	5.87	1.80	4.00	3.21	2.70	1.33	6.87	5.69	3.03	9.60	2.28	5.90	3.70	3.65	6.34	5.63	2.60	4.36
Total	99.62	99.57	99.72	100.10	100.08	99.40	100.54	100.62	99.89	100.66	99.69	99.85	100.03	100.10	100.06	99.67	99.76	99.96
Sc	26.0	27.0	18.0	20.0	25.0	16.0	25.0	18.0	23.0	17.0	33.0	15.0	25.0	34.0	20.0	28.0	27.0	23.4
V	213.0	200.0	239.0	276.0	246.0	226.0	174.0	237.0	225.0	166.0	242.0	158.0	237.0	240.0	224.0	228.0	230.0	221.2
Cr	401.0	363.0	287.0	151.0	328.0	292.0	288.0	375.0	353.0	367.0	447.0	337.0	385.0	317.0	344.0	409.0	326.0	339.4
Ni	284.0	297.0	135.0	115.0	241.0	256.0	218.0	255.0	286.0	568.0	291.0	130.0	269.0	169.0	197.0	285.0	232.0	248.7
Y	29.7	27.2	27.9	29.5	27.2	28.9	24.1	25.2	27.1	20.9	25.5	19.2	24.8	25.8	25.2	24.3	27.9	25.9
Rb	17.1	19.2	17.2	4.8	17.4	17.4	1.7	1.8	17.1	9.3	21.7	37.2	17.8	15.7	18.0	14.5	16.4	15.6
Sr	967.0	624.0	411.0	826.0	468.0	614.0	303.0	513.0	513.0	224.0	573.0	94.2	595.0	411.0	305.0	426.0	443.0	488.8
Ba	861.0	470.0	428.0	683.0	666.0	431.0	197.0	511.0	524.0	221.0	514.0	445.0	719.0	361.0	349.0	363.0	581.0	489.7
Zr	172.0	172.0	143.0	247.0	155.0	176.0	96.5	140.0	211.0	85.8	156.0	168.0	139.0	125.0	119.0	119.0	149.0	151.4
Nb	45.4	42.1	26.7	65.5	32.1	41.2	16.4	31.4	40.7	20.3	39.2	22.6	36.5	25.5	23.3	25.2	29.8	33.2
Ga	19.0	19.1	21.2	18.6	20.6	20.2	19.3	19.6	20.9	14.2	19.1	17.7	18.0	20.7	20.6	20.1	20.3	19.4
Pb	3.9	5.3	3.6	6.5	3.4	4.8	3.1	3.4	5.7	2.3	4.5	2.8	4.0	2.9	2.9	2.8	4.6	3.9
Th	11.6	11.9	8.9	13.5	9.7	10.9	6.0	8.8	11.1	6.2	11.2	7.1	10.8	8.3	7.1	7.7	9.1	9.4
U	3.9	6.1	6.5	5.2	6.1	6.1	5.8	5.3	5.7	6.5	6.3	7.0	5.6	5.9	6.0	6.0	6.0	5.9
Hf				5.92						2.05		3.70	3.86					3.88
Ta				3.36						1.01		1.43	2.06					1.97
Mg no.	0.58	0.62	0.60	0.56	0.63	0.60	0.63	0.68	0.62	0.70	0.66	0.60	0.67	0.60	0.67	0.62	0.64	0.63

Fe_2O_3* is total iron presented as Fe_2O_3, and Mg no. = (molar $Mg/(Mg+Fe^{2+})$) assuming $Fe^{3+}/Fe^{2+} = 0.15$.

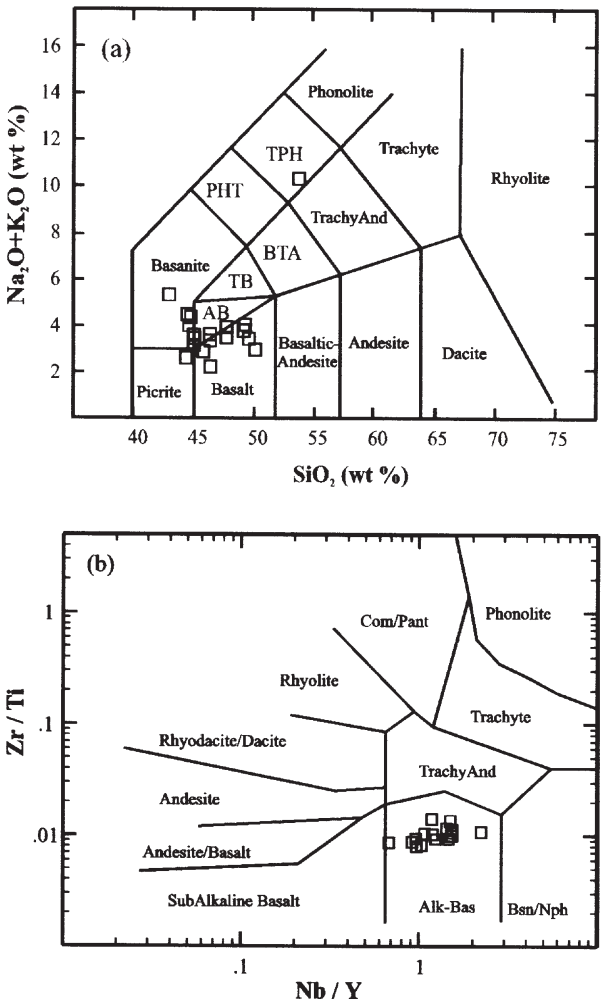

Figure 4. (a) Total alkali–silica (TAS) diagram (after Le Bas *et al.* 1986 and Le Bas & Streckeisen, 1991) showing the classification of the Lebanese Mesozoic mafic volcanic rocks (recalculated on an anhydrous basis). Fields are: TPH, tephriphonolite; PHT, phonotephrite; TB, trachybasalt; AB, alkali basalt; BTA, basaltic trachyandesite. (b) Zr/Ti v. Nb/Y diagram (after Winchester & Floyd, 1977) showing that all data points of the Lebanese Mesozoic basalts plot in the field of alkali basalt.

ratios, such as La/Nb (0.66) and Zr/Nb (4.75), similar to HIMU-OIB (e.g. the St Helena alkali basalts that exhibit La/Nb = 0.69 and Zr/Nb = 4.5: Weaver, 1991). The investigated rocks, with their (Ti/V) ratios ranging from 65 to 90, belong to the alkaline basalt group of Shervais (1982).

Variation diagrams of selected major-elements versus Zr (Fig. 5) indicate that P_2O_5, TiO_2, alkalis and total iron (as Fe_2O_3) increase gradually with increasing Zr, whereas Al_2O_3 remains somewhat constant. Variations of selected trace-elements versus Zr indicate that most trace elements show well-defined trends; Sr, Pb, Th, Nb and Y show a gradual increase with increasing Zr (Fig. 5).

Since Zr and Y are incompatible in the main fractionating phases of basaltic magmas (olivine, pyroxene and plagioclase), the Zr/Y ratio is not normally affected by moderate amounts of fractional crystallization. The variation of (Zr/Y) with Zr or with FeO could be used to illustrate petrogenetic processes such as fractional crystallization or partial melting. As Zr is more incompatible in mantle phases than Y (Nicholson & Latin, 1992), the Zr/Y ratios (and also the concentrations of FeO) tend to be higher when the degree of melting is small. The linear positive variations of Zr/Y which decrease with decreasing Zr (Fig. 6) suggest that the Lebanese basaltic magmas were generated by variable degrees of partial melting. This diagram indicates also that all data points plot exclusively in the field of within-plate basalts (e.g. Pearce & Norry, 1979), consistent with an extensional tectonic regime (see Section 6.d).

5.b. The rare earth elements

The concentrations of the rare earth elements (REE) in representative samples of the Lebanese Mesozoic alkali basalts are given in Table 3, and the primitive mantle-normalized REE patterns are presented in Figure 7a. The rocks are enriched in the REE, with total REE ranging from 79–193 ppm. Overall, the REE patterns are parallel to subparallel, and are generally strongly LREE enriched ($(La/Yb)_N$ = 11), typical of OIB-type alkali basalts (e.g. Sun & McDonough, 1989; Wittke & Mack, 1993; Coulon *et al.* 1996).

The primitive mantle-normalized incompatible element profiles of the Lebanese Mesozoic alkali basalts (Fig. 7b) show that the rocks are enriched in the incompatible elements and strongly enriched in U, Pb and Ti, but exhibit moderate depletion in Rb and K. These trace-element profiles are typical of OIB and continental intraplate alkaline basaltic rocks which are generally characterized by higher concentrations of the HFSE than the large ion lithophile elements (LILE; as K and Rb: Thompson *et al.* 1984; Sun & McDonough, 1989; Francis, 1995).

5.c. Rb–Sr and Sm–Nd isotopes

The Sr and Nd isotopic compositions of three representative samples from the Lebanese Mesozoic alkali basalts are given in Table 4. In terms of the $^{87}Sr/^{86}Sr$ isotopic composition, the Lebanese basalts range from 0.702971 ± 2 to 0.703669 ± 2, and their $^{143}Nd/^{144}Nd$ values range from 0.512826 ± 1 to 0.512886 ± 1. It should be noted that the slightly wide range of the Sr-isotopic composition is probably the result of post-eruption alteration; other elements, such as Ba, may have also been affected by alteration. However, the Sr–Nd isotopic compositions of basalts from Israel and Syria (as reported in Laws & Wilson, 1997) are indistinguishable from those of the Lebanese basaltic rocks obtained as part of this study. Age-corrected Sr–Nd isotopic compositions of the Lebanese Mesozoic

https://doi.org/10.1017/S0016756802006829 Published online by Cambridge University Press

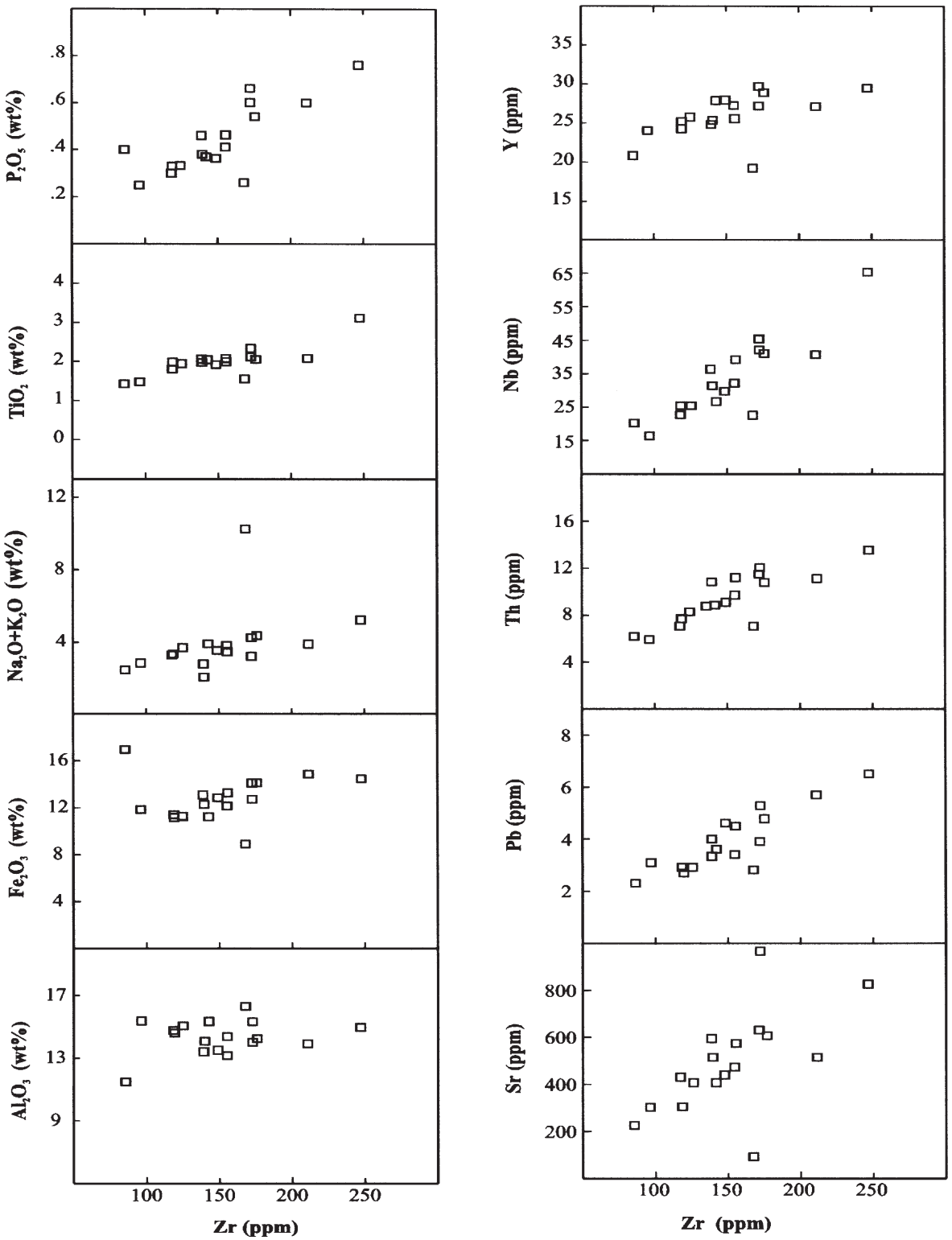

Figure 5. Variations of selected major and trace elements v. Zr. Major elements used in this diagram were recalculated on an anhydrous basis.

alkali basalts (corrected for the approximate age of emplacement, 120 Ma), are plotted in Figure 8, with data for other alkali basaltic suites from the Cameroon Line, St Helena, the Benue Trough of Nigeria, and from the Middle East.

Also plotted in this diagram are the compositions of the various mantle reservoirs (EMI, EMII, HIMU and N-MORB), taken from Hart (1988). For each mantle reservoir, the field shown by the arrow corresponds to the composition of the reservoir at 120 Ma. It should be noted that HIMU ('high μ') refers to a high $^{238}U/^{204}Pb$ (μ) mantle end-member, and has the

https://doi.org/10.1017/S0016756802006829 Published online by Cambridge University Press

Table 3. Rare earth element (REE) compositions (in ppm) of the Mesozoic basalts of Lebanon

Sample	AR-9	AR-33	AR-37	AR-39	Average
La	37.43	13.44	15.71	25.04	22.91
Ce	77.49	29.78	31.80	50.46	47.38
Pr	9.46	3.72	3.82	6.15	5.79
Nd	38.61	16.08	15.89	25.96	24.14
Sm	8.24	3.73	3.64	6.08	5.42
Eu	2.63	1.26	0.79	2.02	1.68
Gd	7.23	3.59	3.46	5.78	5.02
Tb	0.99	0.52	0.48	0.81	0.70
Dy	5.35	2.95	2.70	4.44	3.86
Ho	0.97	0.56	0.48	0.82	0.71
Er	2.46	1.46	1.26	2.06	1.81
Tm	0.30	0.20	0.16	0.26	0.23
Yb	1.88	1.16	0.99	1.45	1.37
Lu	0.26	0.17	0.13	0.21	0.19
ΣREE	193.30	78.60	81.30	131.50	121.18

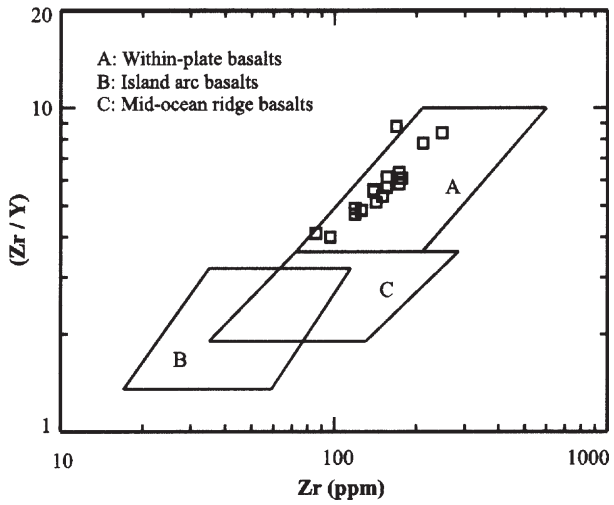

Figure 6. Zr/Y v. Zr variation diagram for the Lebanese Mesozoic basaltic rocks; note the linear positive variations of Zr/Y which decrease with decreasing Zr (see text for details). The diagram indicates also the within-plate nature of these basalts (fields are after Pearce & Norry, 1979).

lowest $^{87}Sr/^{86}Sr$ of any OIB (Hofmann, 1997), which is thought to be derived from subducted basaltic oceanic crust. EMI ('enriched mantle 1') and EMII ('enriched mantle 2') types of OIB may represent the addition of small amounts of subducted sediments: pelagic in the case of EMI and terrigenous in the case of EMII (Weaver, 1991; Hofmann, 1997). Examples of HIMU-OIB are St Helena, Bouvet, Ascension, Austral Islands, Balleny Islands and the Azores, of EMI-OIB are Tristan da Cunha, Gough, Kerguelen and Pitcairn, and of EMII-OIB are Society Islands, Samoa, Tutuila and Upolu (Weaver, 1991; Hofmann, 1997).

The Lebanese Mesozoic alkali basalts exhibit isotopic compositions similar to HIMU-OIB (relatively high initial $^{143}Nd/^{144}Nd$ and low initial $^{87}Sr/^{86}Sr$ isotopic ratios), and are thus distinct from EMI-OIB and EMII-OIB (e.g. Weaver, 1991; Wilson, 1993). Figure 8 shows that the investigated rocks are also isotopically similar to the plume-related St Helena alkali basalts (Staudigel *et al.* 1984; Hofmann, 1997), to Mesozoic alkali basalts from other parts of the Middle East (Laws & Wilson, 1997), to the Cameroon Line basalts (Halliday *et al.* 1988; 1990; Lee *et al.* 1994), and to the Benue Trough alkaline basalts of Nigeria (Coulon *et al.* 1996).

Table 4. Sr and Nd isotopic composition of representative samples from the Mesozoic alkali basalts of Lebanon

Sample	AR-9	AR-20	AR-39	Average
$^{87}Rb/^{86}Sr$	0.017	0.016	0.087	0.040
$^{87}Sr/^{86}Sr$	0.703669	0.703528	0.702971	0.703389
$^{147}Sm/^{144}Nd$	0.1259	0.1619	0.1393	0.1424
$^{143}Nd/^{144}Nd$	0.512886	0.512826	0.512848	0.512853

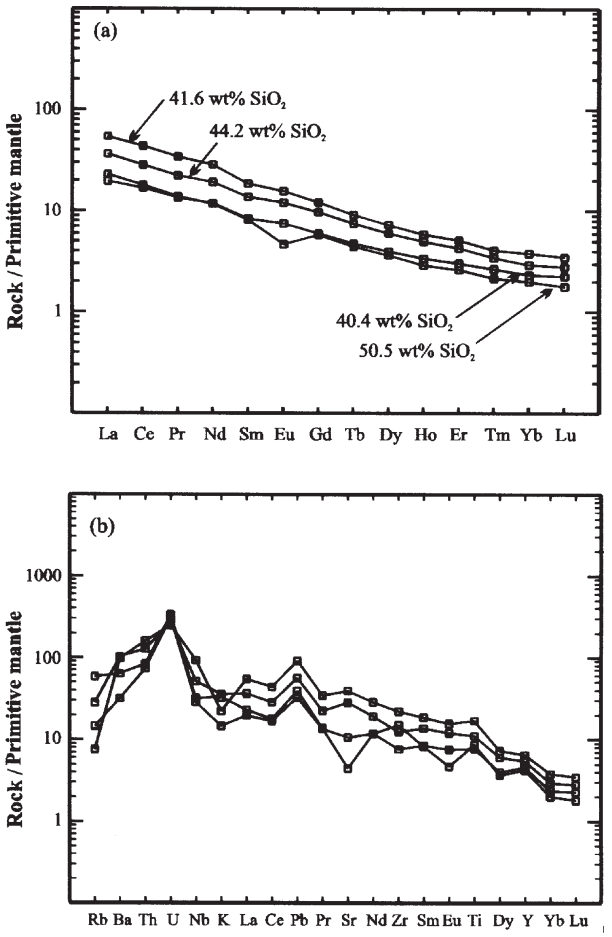

Figure 7. (a) Primitive mantle-normalized rare earth element patterns of representative samples from the Lebanese Mesozoic alkali basalts. The REE patterns are strongly fractionated and are generally parallel to subparallel. Normalization values used are taken from Sun & McDonough (1989). (b) Primitive mantle-normalized incompatible element patterns for the Lebanese Mesozoic alkali basalts. Normalization values used are same as in Figure 7a. The patterns are generally uniform and conformable.

https://doi.org/10.1017/S0016756802006829 Published online by Cambridge University Press

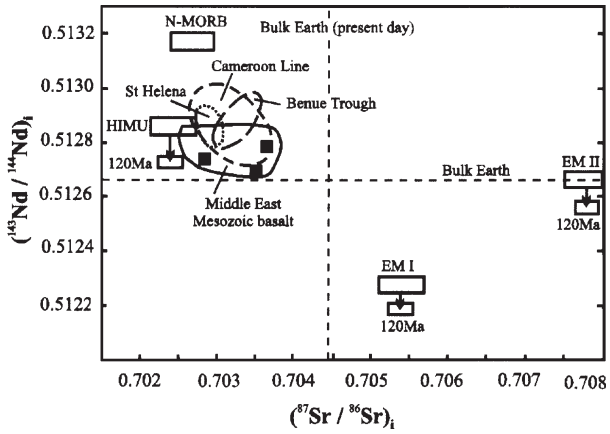

Figure 8. $(^{87}Sr/^{86}Sr)_i$ v. $(^{143}Nd/^{144}Nd)_i$ ratios for the Lebanese Mesozoic basaltic rocks (filled squares) corrected for average age of emplacement (120 Ma). Compositions of EMI, EMII, HIMU and N-MORB are from Hart (1988). For each of these mantle reservoirs, the field shown by the arrow corresponds to the composition of the reservoir at 120 Ma; the evolution of the $^{143}Nd/^{144}Nd$ ratio of the mantle reservoirs through time is the most sensitive to radiogenic growth over the period of time considered (Coulon *et al.* 1996). This evolution has been estimated assuming a μ value of 22 for the HIMU reservoir (Chauvel, Hofmann & Vidal, 1992), 8 for the other reservoirs, and a $^{147}Sm/^{144}Nd$ of 0.222 for the depleted mantle (Ben Othman, Fourcade & Allègre, 1984). Fields for St Helena from Staudigel *et al.* (1984), Cameroon Line from Halliday *et al.* (1988) and Lee *et al.* (1994), the southern Benue Trough alkali basalts from Coulon *et al.* (1996) and the Middle East Mesozoic basalts from Laws & Wilson (1997). See text for details.

6. Discussion

6.a. Depth of melting and a possible plume-source

As shown in Figure 8, the Sr–Nd isotopic composition of the investigated rocks is similar to that of HIMU-OIB. Other parts of the Mesozoic alkali basalt province of the Middle East, namely the Mount Hermon basalts and the Maktesh Ramon basalts of Israel, also exhibit isotopic compositions similar to those of HIMU-OIB (Laws & Wilson, 1997). The HIMU-OIB lavas of the Cameroon Line, which are also isotopically similar to the investigated basalts (cf. Fig. 8), were interpreted to represent small degrees of partial melting of upper mantle material caused by the emplacement of a plume in the upper mantle 125 Ma ago (Halliday *et al.* 1990). In terms of their Zr, Nb and Y compositions (Fig. 9a), the investigated basaltic rocks geochemically resemble plume-related MORB (P-MORB), as they exhibit relatively higher concentrations of Nb and Zr, but lower concentrations of Y than transitional- or normal-MORB (T-MORB or N-MORB; Menzies & Kyle, 1990; Melluso *et al.* 1995). Thus, trace element and isotopic data suggest that the Lebanese basaltic rocks may be derived from a plume source. Figure 9a shows also that all data points of the investigated basalts plot within the field of HIMU-OIB (delineated using data of the St Helena, Bouvet and Ascension ocean islands which are given in Weaver *et al.* 1987). Furthermore, the Lebanese Mesozoic alkali basalts exhibit elemental ratios ((Zr/Nb) = 4.75, (La/Nb) = 0.66, (Ba/Th) = 51 and (Rb/Nb) = 0.51, on average) similar to those characteristic of HIMU-OIB (Sun & McDonough, 1989; Weaver, 1991).

Bradshaw & Smith (1994) and Smith *et al.* (1999) suggested that, since high field strength elements (such as Nb) are depleted in the lithospheric mantle relative to the light rare earth elements (such as La), high Nb/La ratios (approximately > 1) indicate an OIB-like asthenospheric mantle source for basaltic magmas, and lower ratios (approximately < 0.5) indicate a lithospheric mantle source. The Nb/La and La/Yb ratios (averages of 1.54 and 16.2, respectively) are consistent with an asthenospheric mantle (OIB-like) source (Fig. 9b), and all data points of the investigated basalts plot within the field of HIMU-OIB, as also observed in Figure 9a.

The presence of residual garnet in the source region is inferred from the primitive mantle-normalized REE patterns; the most diagnostic feature of residual garnet is the depletion of heavy rare earth elements (HREE) relative to light rare earth elements (LREE; cf. Fig. 7a) owing to their strong partitioning into garnet (Wallace & Carmichael, 1992; Spath, Le Roex & Duncan, 1996). The presence of garnet as residue in the source is also inferred by the value of the Dy/Yb ratio which is higher than that of chondrite (Dy/Yb = 1.57); the Lebanese Mesozoic alkali basalts have an average Dy/Yb ratio of 2.81. These rocks also have $(Tb/Yb)_N$ ratios ranging between 1.91 and 2.39, which are comparable to those of the alkali basalts of Hawaii ($(Tb/Yb)_N$ range from 1.89 to 2.45); the Hawaiian basalts are also considered to have been derived from a garnet lherzolite mantle source (Frey *et al.* 1991; McKenzie & O'Nions, 1991).

According to Bhat, Le Fort & Ahmad (1994), residual garnet would selectively limit Yb contents in the melt, but increases that of La. High La/Yb ratios (16.2, on average) and low Yb (1.37 ppm, on average) in the Lebanese basaltic suite confirm that garnet was a residual phase in the mantle source during magma generation. The (CaO/Al_2O_3) ratio can be used to characterize the mantle source region (Haase & Devey, 1994). Primitive mantle is inferred to have a (CaO/Al_2O_3) ratio of 0.79–0.81 (Zindler & Hart, 1986; Sun & McDonough, 1989) and the average ratio in garnet lherzolite mantle xenoliths is 0.74 (Maaløe & Aoki, 1977). The Lebanese Mesozoic alkali basalts have (CaO/Al_2O_3) ratios ranging between 0.59 and 0.85, with an average of 0.72, similar to that of garnet lherzolites.

Using the study of Ellam (1992) on the estimation of depths of melt segregation, curves corresponding to the Ce, Sm and Yb concentrations of the Lebanese

https://doi.org/10.1017/S0016756802006829 Published online by Cambridge University Press

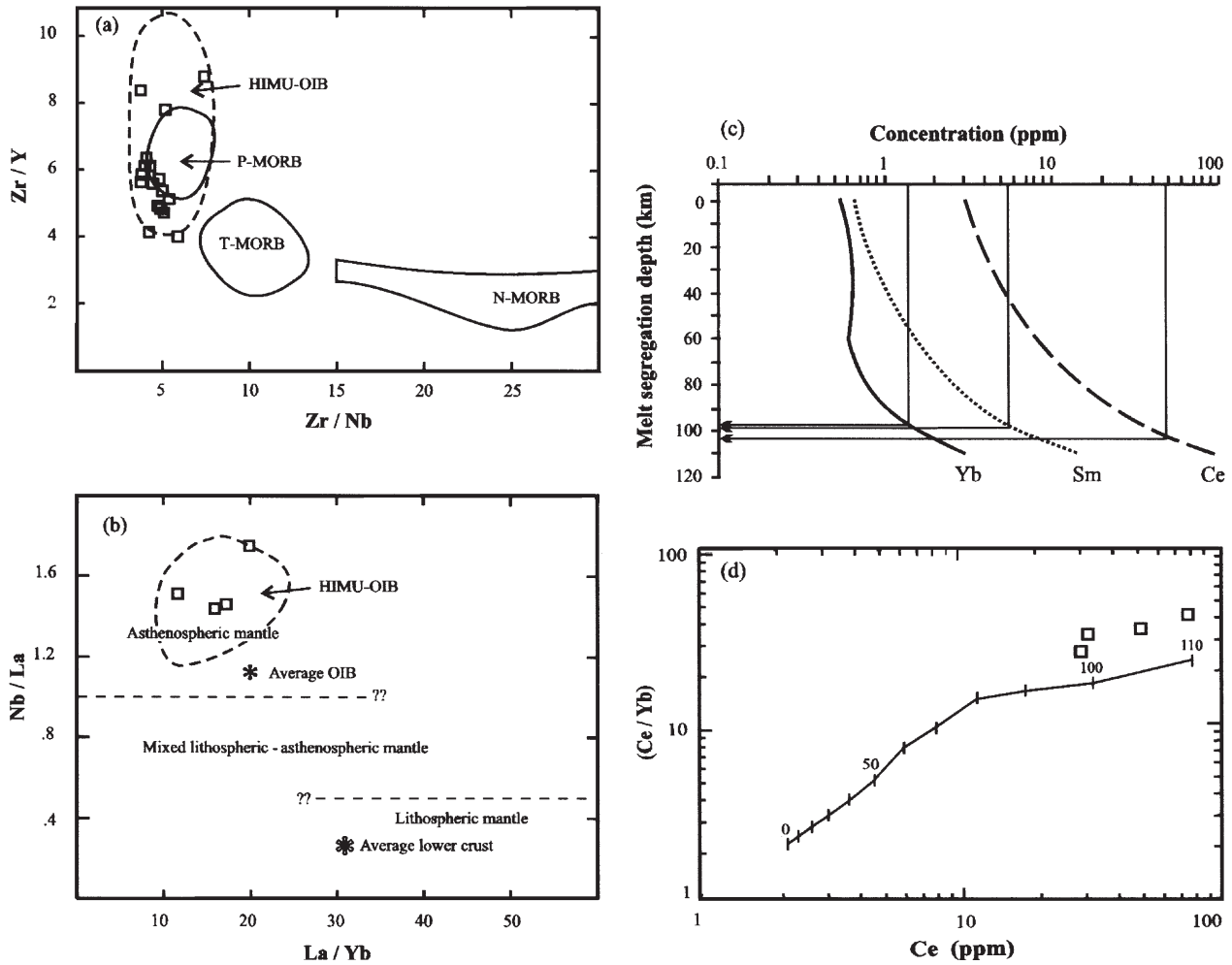

Figure 9. (a) Zr/Y v. Zr/Nb diagram showing that the Lebanese Mesozoic alkali basalts plot within the field of HIMU-OIB, and in or near the field of fertile, plume-related MORB (P-MORB). The other fields are transitional MORB (T-MORB) and normal MORB (N-MORB) and are taken from Menzies & Kyle (1990). The field of HIMU-OIB is delineated based on data of the St Helena, Bouvet and Ascension ocean islands, reported in Weaver *et al.* (1987). See text for details. (b) Nb/La v. La/Yb variation diagram. The composition of the Lebanese Mesozoic alkali basalts (low La/Yb and high Nb/La) suggests an OIB-like asthenospheric mantle source. Average OIB is after Fitton, James & Leeman (1991), and average lower crust (representing average of six lower crustal granulite xenoliths) is after Chen & Arculus (1995). Dashed lines separating fields of the asthenospheric, lithospheric and mixed mantle are plotted based on data given in Smith *et al.* (1999). The field of HIMU-OIB is delineated based on data of the St Helena, Bouvet and Ascension ocean islands, reported in Weaver *et al.* (1987), and assuming Yb = Tb ÷ 0.5. (c) Model Ce, Sm and Yb concentrations in melts generated by partial melting and ranges of final melt segregation depths (model curves are after Ellam, 1992). The average compositions of the Lebanese Mesozoic basalts (marked by vertical lines) indicate melt segregation at depths of about 97 to 103 km. (d) Ce/Yb v. Ce diagram showing the range of melt segregation depth of the Lebanese basalts; tick marks on model curves indicate depth of final melt segregation in 10 km increments, and are after Ellam (1992).

Mesozoic alkali basalts (Fig. 9c) indicate a melt segregation depth ranging from about 97 to 103 km. As pointed out by Ellam (1992), REE ratios such as Sm/Yb and Ce/Yb offer sensitive indicators of changing lithospheric thickness because they will not be radically affected by fractional crystallization. In the Ce/Yb v. Ce diagram (Fig. 9d), data for the Lebanese Mesozoic alkali basalts indicate a melt segregation depth of about 100–110 km (that is, within the garnet lherzolite zone), consistent with an asthenospheric mantle source as indicated in Figure 9b. It should be noted that the transition from garnet to spinel peridotite takes place between a depth of about 60 to 80 km for normal mantle and about 80 to 100 km within hot mantle plumes (McKenzie & O'Nions, 1991; Lassiter, DePaolo & Mahoney, 1995).

6.b. Petrogenetic considerations: role of partial melting

Many alkali basaltic suites are known to be of a deep mantle origin, and related to mantle plumes, but with other suites having lithospheric origin (e.g. Frey *et al.* 1991; Hoernle & Schmincke, 1993; Coulon *et al.* 1996; Haase, Stoffers & Garbe-Schönberg, 1997; Gibson *et al.* 1997; Abdel-Rahman & Kumarapeli, 1999; Frey *et al.* 2000). However, they are extremely diverse geo-

https://doi.org/10.1017/S0016756802006829 Published online by Cambridge University Press

chemically and were derived from diverse mantle sources (e.g. White, 1985; Allègre *et al.* 1987; Hart, 1988; Weaver, 1991). The nature of the mantle source material, whether it is dominated by recycled oceanic or continental crust, or by recycled sedimentary components, and the processes associated with melting and migration of melt, determine the composition of the basaltic lavas. Baker (1973) and Haase (1996) related variations in the composition of intra-plate basalts to the age of the underlying lithosphere. According to Haase, Stoffers & Garbe-Schönberg (1997), this relationship is probably due to an increase in the depth of the zone of partial melting as the lithosphere thickens with age, irrespective of whether the volcanoes are of plume (Ellam, 1992) or non-plume origin (Batiza, 1980).

Several geochemical parameters have been used to assess the role of petrogenetic processes such as fractional crystallization and partial melting in the evolution of mafic lavas. For example, during partial melting processes, the highly/moderately incompatible element ratios (such as Ba/Y, Ba/Zr and P_2O_5/TiO_2), are known to decrease with increasing degrees of partial melting (Pankhurst, 1977). This author demonstrated that partial melting is still by far the most efficient process for fractionating highly/moderately incompatible element ratios. The linear positive trends between these elemental ratios and the concentrations of the highly incompatible elements obtained for the Lebanese lavas (Fig. 10a,b,c) suggest that partial melting may have been the dominant petrogenetic process. The ratio of an element (X) incompatible during melting to Al_2O_3 (which is usually buffered by residual garnet) typically decreases systematically with increasing degrees for partial melting (Hoernle & Schmincke, 1993). The variations of Zr/Al_2O_3, Nb/Al_2O_3 and Sr/Al_2O_3 v. P_2O_5/Al_2O_3 (Fig. 10d,e,f) produced well-defined linear trends, mostly passing through the origin, which is indicative of the significant role of partial melting processes (e.g. Hoernle & Schmincke, 1993) in producing the range of magma chemistry observed in the Lebanese basaltic suite.

Overall, the geochemical features described above indicate that the source of the Lebanese Mesozoic alkali basalts was a fertile, garnet-bearing, lherzolitic mantle material, and that the magmas were produced by variable degrees of partial melting. To test this hypothesis, partial melting modelling was performed, using the batch melting equations of Shaw (1970). The calculations were done using two model source compositions, those of a primitive mantle taken from Sun & McDonough (1989) and a mixed (50% primitive–50% depleted) mantle source of McKenzie & O'Nions (1991). Residual mineralogy varied between those of spinel and garnet lherzolite. Spinel, garnet and clinopyroxene were assumed to decrease in abundance linearly with increasing degrees of partial melting, as they are typically consumed at less than 25% partial melting (McKenzie & O'Nions, 1991; Lassiter, DePaolo & Mahoney, 1995). Model proportions and melting proportions used are given in Table 5, and are similar to those used in other partial melting calculations (e.g. Hanson, 1980; McKenzie & O'Nions, 1991; Witt-Eickschen & Kramm, 1997). Modelling was performed using three different mantle mineral assemblages: spinel lherzolite, garnet lherzolite and spinel-garnet lherzolite, for both a primitive and a mixed source composition. The partition coefficients used are from McKenzie & O'Nions (1991).

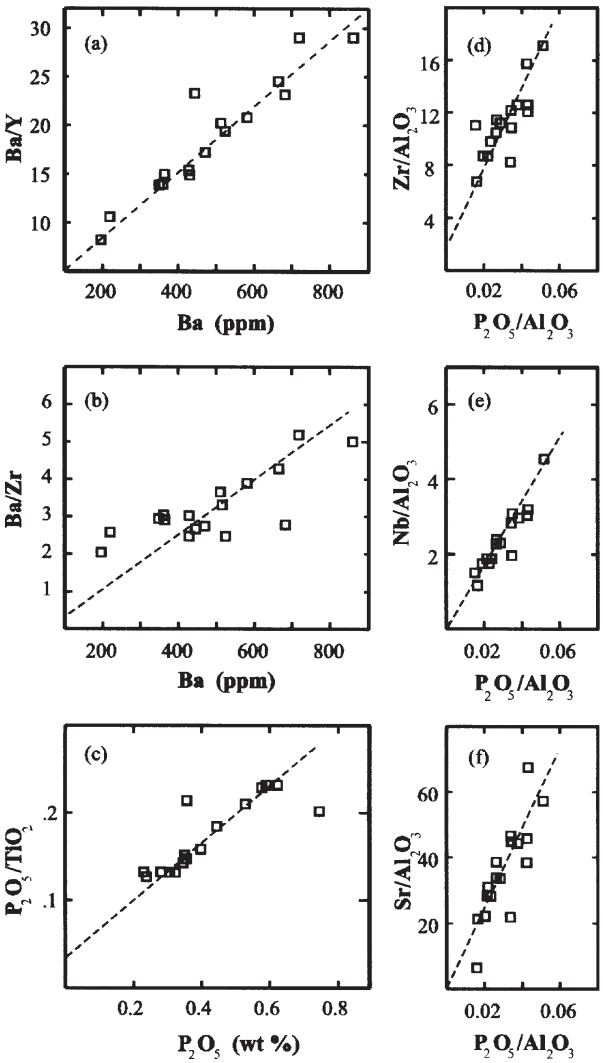

Figure 10. (a, b, c) Plots showing highly/moderately incompatible element ratios v. highly incompatible element concentrations for the Lebanese Mesozoic alkali basalts. Zr/Al_2O_3, Nb/Al_2O_3 and Sr/Al_2O_3 v. P_2O_5/Al_2O_3 diagrams (d, e, f, respectively) for the Lebanese Mesozoic alkali basalts. See text for details.

Partial melting calculations were performed for 0.5%, 1.5% and 3% partial melting. The results of the mantle melt modelling (presented in Table 5 and Fig. 11) show that melting of a spinel-bearing source overestimates the HREEs, and melting of a mixed source

https://doi.org/10.1017/S0016756802006829 Published online by Cambridge University Press

Table 5. Model parameters and results of batch partial melting calculations using various mineralogical and chemical compositions of primitive and mixed mantle sources

	Starting mode			Melt mode		
Phase	a	b	c	a	b	c
Olivine	0.570	0.550	0.55	0.15	0.05	0.15
Opx	0.235	0.220	0.22	0.15	0.05	0.15
Cpx	0.160	0.160	0.16	0.35	0.30	0.35
Garnet	0.000	0.035	0.07	0.00	0.30	0.35
Spinel	0.035	0.035	0.00	0.35	0.30	0.00

REE	1	2	3	4	5	6	7	8	9	10	11	12	13	14	15	16	17	18	19
La	25.93	15.52	9.69	25.38	15.32	9.61	25.39	15.32	9.61	47.13	28.21	17.61	46.14	27.85	17.46	46.15	17.47	27.86	22.91
Ce	48.60	33.74	23.13	47.14	33.03	22.80	46.38	32.69	22.66	81.31	56.44	38.69	78.86	55.26	38.14	77.59	37.91	54.69	47.38
Pr	5.92	4.52	3.34	5.59	4.34	3.25	5.35	4.20	3.17	9.00	6.88	5.08	8.51	6.60	4.946	8.13	4.83	6.39	5.79
Nd	23.27	18.98	14.86	21.75	18.04	14.30	20.51	17.18	13.82	33.24	27.10	21.23	31.07	25.71	20.43	29.30	19.74	24.54	24.14
Sm	6.55	5.54	4.50	5.72	4.98	4.16	5.08	4.50	3.83	8.95	7.57	6.15	7.82	6.80	5.68	6.95	5.24	6.15	5.42
Eu	2.10	1.83	1.52	1.78	1.59	1.38	1.54	1.40	1.24	2.87	2.49	2.08	2.43	2.18	1.88	2.10	1.69	1.92	1.68
Gd	7.62	6.60	5.50	5.92	5.37	4.71	4.82	4.47	4.02	10.38	8.98	7.48	8.06	7.31	6.42	6.56	5.48	6.08	5.02
Tb	1.35	1.18	0.99	0.957	0.88	0.79	0.73	0.69	0.64	1.80	1.57	1.32	1.27	1.18	1.06	0.97	0.85	0.92	0.70
Dy	8.59	7.55	6.395	5.534	5.22	4.82	4.04	3.89	3.69	11.57	10.17	8.60	7.45	7.03	6.49	5.44	4.97	5.24	3.86
Ho	2.03	1.77	1.49	1.11	1.07	1.01	0.75	0.74	0.71	2.67	2.33	1.96	1.46	1.40	1.32	0.99	0.94	0.97	0.71
Er	5.92	5.16	4.33	2.82	2.75	2.66	1.83	1.81	1.78	7.90	6.90	5.79	3.77	3.68	3.55	2.44	2.38	2.42	1.81
Tm	0.91	0.79	0.66	0.34	0.34	0.34	0.21	0.21	0.21	1.20	1.05	0.88	0.45	0.45	0.45	0.27	0.28	0.28	0.23
Yb	5.80	5.07	4.27	1.83	1.86	1.90	1.07	1.08	1.11	7.95	6.95	5.85	2.51	2.55	2.61	1.46	1.52	1.49	1.37
Lu	0.86	0.76	0.64	0.22	0.23	0.24	0.12	0.13	0.13	1.146	1.00	0.85	0.29	0.30	0.32	0.16	0.17	0.17	0.19

Calculated melts produced by 0.5%, 1.5%, and 3% batch partial melting are no. 1 to no. 18, and no. 19 is the measured, average concentration of the Lebanese Mesozoic basalts. The starting mode, melt mode, and mantle source type used to produce each of the calculated melts are as follows:
Melt nos 1–3: starting mode a, melt mode a, mixed source, for 0.5, 1.5, and 3.0% melting, respectively;
Melt nos 4–6: starting mode b, melt mode b, mixed source, for 0.5, 1.5, and 3.0% melting, respectively;
Melt nos 7–9: starting mode c, melt mode c, mixed source, for 0.5, 1.5, and 3.0% melting, respectively;
Melt nos 10–12: starting mode a, melt mode a, primitive source, for 0.5, 1.5, and 3.0% melting, respectively;
Melt nos 13–15: starting mode b, melt mode b, primitive source, for 0.5, 1.5, and 3.0% melting, respectively;
Melt nos 16–18: starting mode c, melt mode c, primitive source, for 0.5, 3, and 1.5% melting, respectively.
The composition of the calculated melt no. 18 (produced by 1.5 percent melting of garnet lherzolite of a primitive mantle source) closely matches that of the measured average composition of the Lebanese Mesozoic basalts (no. 19). See text for details.

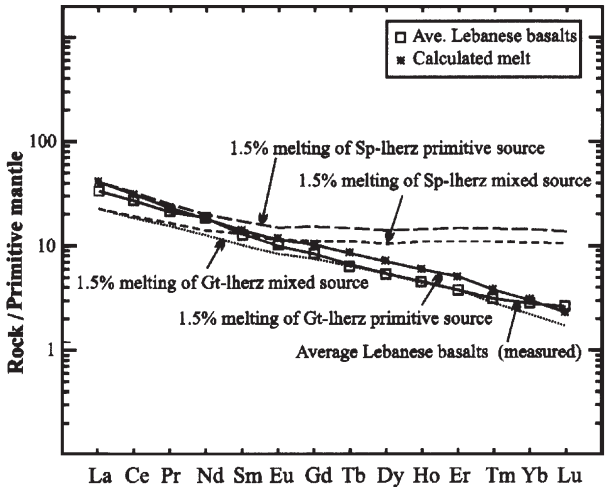

Figure 11. Calculated REE patterns for melts derived by batch partial melting of a primitive mantle composition with REE concentrations from Sun & McDonough (1989) and of a mixed source (50% primitive/50% depleted mantle) with REE concentrations from McKenzie & O'Nions (1991). The mantle mineral assemblages and melting proportions used are listed in Table 5. The calculations were made using the Kds of McKenzie & O'Nions (1991), for degrees of partial melting (F) = 0.5%, 1.5% and 3%. Normalization values used are taken from Sun & McDonough (1989). The calculated REE pattern produced by 1.5% melting of a primitive garnet lherzolite source matches that of the average Lebanese Mesozoic alkali basalts.

yields much lower LREE concentrations. Thus, neither depleted nor mixed primitive/depleted mantle material represents the mantle source for the Lebanese basalts; in this source garnet is a required phase.

The REE pattern of the calculated liquid produced by 1.5% batch partial melting of garnet lherzolite (of a primitive mantle composition) produces the best fit, as it closely matches that of average Lebanese Mesozoic alkali basalts (Fig. 11). Although data for the calculated model liquid and that of the observed melt match closely, Frey, Green & Roy (1978) considered that up to a 15% difference between calculated and observed melts represented excellent agreement. It should be noted that the degree of partial melting (1.5%) of garnet lherzolite to produce the investigated lavas is generally low for plume-related basalts. However, this is consistent with the relatively small volume of these lavas, compared to plume-related basalts from other localities (e.g. Abdel-Rahman & Kumarapeli, 1999). The relatively small volume of the erupted Mesozoic basaltic rocks of Lebanon suggests that these basalts do not represent 'trap' lavas, but rather reflects that they were related to a thermal mantle anomaly.

6.c. Nature of the Levantine crust and role of crustal contamination

Two main hypotheses have been suggested for the nature of the Levantine crust in the Eastern Mediterranean region, proposing either an oceanic or a continental origin. Based on geological and geophysical data, Hirsch *et al.* (1995) suggested that the crust is made up of a 15 km thick sedimentary succession overlying a thinned crust of Precambrian continental basement. Knipper & Sharaskin (1994) suggested that this Precambrian igneous–metamorphic continental basement could have thinned because of a change in its physical properties as an exceedingly thick pile of overlying, mostly Mesozoic, sedimentary rocks accumulated.

In support of the oceanic crust hypothesis, several authors including Freund *et al.* (1975) and Ginzburg & Ben-Avraham (1987), argued that crust of the Levant region was developed during periods of Mesozoic rifting and oceanic crust formation. Ben-Avraham (1989) and Ben-Avraham & Ginzburg (1990) used magnetic and gravity data to support this hypothesis. Khair & Tsokas (1999) used gravity data to provide further support to the oceanic crust hypothesis; they suggested that the Levantine crust is made up of about 10 km of Phanerozoic sedimentary deposits overlying a 12 km thick, igneous–metamorphic oceanic-like basement complex. Khair & Tsokas (1999) estimated that the Moho occurs at a depth of about 20 to 28 km below sea level. If correct, the presence of such a very thin, mafic, oceanic-like crust in the Eastern Mediterranean may account for the lack of significant crustal contamination in the Lebanese Mesozoic basalts.

Certain chemical parameters that are usually strongly affected by crustal contamination can be used to assess the degree of this contamination. For example, basaltic rocks affected by crustal contamination exhibit K/P ratios > 7, La/Ta > 22 and La/Nb > 1.5 (e.g. Hart *et al.* 1989). The low values of such elemental ratios in the Lebanese basalts (K/P, 1.1–4.7; La/Ta, 11–13; La/Nb, 0.57–0.70; Nb/Y, 0.68–1.55; Th/Nb, 0.20–0.36), along with their Sr–Nd isotopic composition, and their low average silica content (44.9 wt% SiO_2), suggest that the magmas were subjected to minimal crustal contamination. Magma ascent may have been rapid enough from the site of partial melting to the surface to escape contamination. As pointed out by Smith *et al.* (1999), the Nd content of most of the lower crustal xenoliths is too low (usually < 10 ppm) to significantly change Nd-isotopic values without adding 70% to 85% lower crustal material. Such large amounts of contamination by crustal material is thermodynamically difficult because a considerable amount of heat is required to assimilate crustal rocks, and the magma would then cool quickly and perhaps 'freeze' in place. Moreover, this would have resulted in the presence of some lower crustal xenoliths within the lava flows, but the Lebanese basaltic flows contain no lower crustal xenoliths. Thus, the geochemical and field characteristics, along with the nature of the Levantine crust, suggest that crustal contamination probably played an insignificant role during magma evolution.

https://doi.org/10.1017/S0016756802006829 Published online by Cambridge University Press

6.d. Geodynamic context of magma emplacement

The Pan-African orogenic event (1100–550 Ma: Abdel-Rahman & Doig, 1987; Abdel-Rahman, 1995) produced the Arabian–Nubian shield portion of Gondwana at a time when Gondwana was undergoing its final amalgamation. Following the termination of this orogeny, an extended phase of extensional tectonics and associated anorogenic magmatism, spanning nearly the entire Phanerozoic eon (550 Ma to Present; Abdel-Rahman & Martin, 1990; Abdel-Rahman & El-Kibbi, 2001), has affected the Pan-African crust in northeastern Egypt, Sinai, Jordan and northwestern Arabia. Garfunkel (1989) and Robertson *et al.* (1991) suggested that the development of a passive continental margin along the northwestern edge of the Arabian Plate in the Eastern Mediterranean region took place throughout Mesozoic time, as micro-continental blocks (present day southern Turkey, Greece and Cyprus) were separated from Gondwana and moved northwards, with the Neotethys ocean opening up behind them. As the continental margin developed, several stages of rifting are believed to have been operative during Mesozoic time.

An early phase of rifting occurred in the Permo-Triassic and produced the passive margin along the Eastern Mediterranean basin; this rifting has been interpreted (Garfunkel, 1989, 1998) to be the result of several faulting and continental break-up phases before Pangaea's complete disintegration. Along the Levant margin, important rifting also occurred in the Jurassic (Garfunkel, 1998). The main phase of volcanism that produced the alkali basalt province of the Middle East (including the Lebanese basalts) occurred during the Jurassic period. Therefore, given its within-plate nature (cf. Fig. 6) and its chemical characteristics, the Lebanese Mesozoic alkali basalts are interpreted to have been developed in an intraplate setting associated with an episode of crustal extension, possibly related to a mantle plume.

The Early Jurassic alkali basalts of northern Israel (known as the 'Asher' volcanic rocks) were interpreted to represent local manifestations of widespread rifting linked to the opening of the Neotethys ocean, which led to the formation of a continental margin along the periphery of the Arabian plate, or the Levant (Garfunkel, 1989; Gvirtzman, Klang & Rotstein, 1992). According to Garfunkel (1989, 1998), Late Jurassic–Early Cretaceous volcanism in Israel (the 'Tayasir' volcanic suite) occurred in an intraplate setting, in which magmatism and uplifting were interpreted to express the activity of a hot spot. Laws & Wilson (1997) related this Late Jurassic–Early Cretaceous volcanic episode to a rifting stage occurring in association with the formation of the Levant margin. The collision of the African–Arabian continent with Eurasia starting in the Late Cretaceous period ended the extensional tectonic regime along the Eastern Mediterranean margin, and induced regional compression in the Levant (Laws & Wilson, 1997).

6.e. Mesozoic and modern analogues

The Lebanese Mesozoic alkali basalts are here compared to two well-documented extension-related basaltic suites: the Benue Trough alkali basalts of Nigeria, and the Boina basaltic rocks of the Afar Rift in Ethiopia. Based on Ar–Ar radiometric age dating, Maluski *et al.* (1995) recognized three periods of magmatic activity in the Benue Trough: the period 147–106 Ma, represented by transitional alkaline lavas; 97–81 Ma, represented by alkaline intrusive rocks; and 68–49 Ma, represented by alkaline and tholeiitic rocks. The Benue Trough lavas are interpreted to have been produced in a continental rift associated with the opening of the equatorial domain of the South Atlantic above the St Helena mantle plume (Wilson, 1993; Coulon *et al.* 1996). The alkali basaltic suite of the Boina centre, Ethiopia (5 Ma), formed in association with the Afar Rift (Barberi *et al.* 1975; Bizouard, Barberi & Varet, 1980), and has been interpreted to be plume-generated (White & McKenzie, 1989). The striking geochemical similarities between the Lebanese Mesozoic alkali basalts and the Nigerian southern Benue Trough alkaline basalts already outlined for Sr–Nd isotopes (cf. Fig. 8), is here confirmed according to the multi-element diagram (Fig. 12). Moreover, these two suites are identical geochemically to the Boina basalts of the Afar Rift (Fig. 12). Other evidence including: (i) the three basaltic suites are typical of within-plate, anorogenic, rift-related lavas, and (ii) magmas of the three suites have

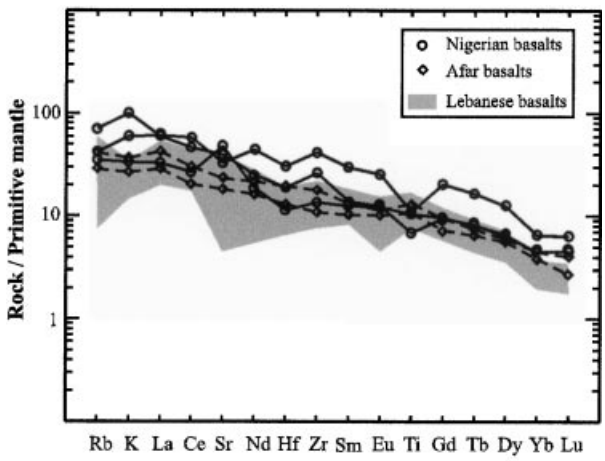

Figure 12. Primitive mantle-normalized incompatible element patterns for representative samples from the Boina Centre basaltic rocks of the Afar Rift, Ethiopia (Barberi *et al.* 1975), and the alkali basalts of the southern Benue Trough of Nigeria (Coulon *et al.* 1996), superimposed on an envelope representing the range of the Lebanese Mesozoic alkali basalts. Normalization values used are those of Sun & McDonough (1989). The three basaltic suites exhibit striking geochemical similarities (see text for details).

https://doi.org/10.1017/S0016756802006829 Published online by Cambridge University Press

been interpreted to be plume-related (White & McKenzie, 1989; Coulon *et al.* 1996; and this study), indicate that the alkali basalts of the southern Benue Trough of Nigeria (147–106 Ma) represent a Mesozoic (contemporaneous) analogue of the Lebanese Mesozoic alkali basalts, whereas the Afar Rift volcanic assemblage of the Boina Centre of Ethiopia appears to represent its modern analogue.

7. Conclusions

(1) The basaltic rocks of Lebanon represent a significant component of a large Mesozoic alkali basaltic province in the Middle East. The rocks are mostly phyric, consisting of about 15–20% olivine ($Fo_{78–91}$), 30–35% clinopyroxene (salite), 40–50% plagioclase ($An_{56–71}$) and opaque phases.

(2) Geochemically, the rocks vary from picrite to basalt (SiO_2, 40.4–50.5 wt%; MgO, 5.1–15.5 wt%), are alkaline in nature (cf. Fig.4b), and are enriched in Ti (1.7–3.7 wt% TiO_2), Zr (86–247 ppm), Nb (16–66 ppm) and Y (19–30 ppm). These features reflect strong affinities to OIB. The primitive mantle-normalized patterns are fractionated ($(La/Yb)_N$ = 11) and conformable.

(3) The Zr, Nb and Y compositions of the Lebanese Mesozoic alkali basalts are typical of those of plume-related magmas. Isotopic ratios ($^{143}Nd/^{144}Nd$, 0.512826–0.512886; $^{87}Sr/^{86}Sr$, 0.702971–0.703669) are similar to those of HIMU-OIB (e.g. the St Helena alkali basalts) recalculated to 120 Ma. The overall chemical characteristics suggest that the Lebanese Mesozoic alkali basalts were derived from a fertile, plume-related, enriched mantle source. Elemental ratios such as K/P (1.1–4.7), La/Nb (0.57–0.70), Nb/Y (0.68–1.55) and Th/Nb (0.20–0.36), suggest that crustal contamination did not play a significant role during magma evolution; the magmas probably experienced very rapid ascent. This is consistent with the nature of the very thin Mesozoic crust of the Eastern Mediterranean region (only about 12 km thick, mafic oceanic-like crust).

(4) Modelling suggests that the magmas were produced by very small degrees of batch partial melting (F = 1.5%) of a garnet-bearing primitive mantle source (garnet lherzolite). A final melt segregation depth is estimated to have occurred at 100–110 km. Melting probably occurred in association with a Mesozoic extensional tectonic regime, as inferred from geochemical and tectonic data.

(5) The Lebanese Mesozoic basalts display the geochemical characteristics of within-plate lavas. This is consistent with the regional geological context in which volcanism was associated with Mesozoic intraplate extension following a period of continental break-up, where Mesozoic micro-continental blocks separated from Gondwana as the Neotethys ocean opened in Jurassic times. The continental rift-related alkali basalts of the Benue Trough of Nigeria represent a Mesozoic (contemporaneous) analogue to the Lebanese Mesozoic alkali basalts, whereas the Boina Centre basalts of the Afar Rift of Ethiopia appear to represent a modern analogue.

Further detailed investigations on the nature of basaltic volcanism in other parts of the Middle East are warranted, in view of their significance in more precisely evaluating the crustal evolution of the Eastern Mediterranean, regional tectonic regimes and Mesozoic mantle dynamics.

Acknowledgements. I thank Mr M. Tubrek and Mr T. Ahmedali for facilitating the acquisition of the X-ray fluorescence and ICP-MS data, respectively. Dr R. Stevensen is thanked for his help in obtaining the Sm–Nd and Rb–Sr isotope data at the UQAM GEOTOP laboratory (Montreal), and Mr G. Poirier for his assistance during the electron microprobe work at McGill University. Discussions with Drs D. Francis, R. Stevensen, S. Schmidberger and T. Simonetti, as well as Mr K. Noubani are appreciated. Mr J. Maalouf is thanked for his assistance during field work. Mr M. Ijreiss and Mrs. H. Nisr provided some technical support. Helpful reviews and valuable comments provided by Dr Marge Wilson, an anonymous referee and by the editors have improved this contribution. Research costs were covered by an AUB-URB grant.

References

Abdel-Rahman, A. M. 1995. Tectonic–magmatic stages of shield evolution: the Pan-African belt in northeastern Egypt. *Tectonophysics* **242**, 223–40.

Abdel-Rahman, A. M. & Doig, R. 1987. The Rb–Sr geochronological evolution of the Ras Gharib segment of the northern Nubian shield. *Journal of the Geological Society, London* **144**, 577–86.

Abdel-Rahman, A. M. & El-Kibbi, M. 2001. Anorogenic magmatism: chemical evolution of the Mount El-Sibai A-type complex (Egypt), and implications for the origin of within-plate felsic magmas. *Geological Magazine* **138**, 67–85.

Abdel-Rahman, A. M. & Kumarapeli, P. S. 1999. Geochemistry and petrogenesis of the Tibbit Hill metavolcanic suite of the Appalachian Fold Belt, Quebec-Vermont: a plume-related and fractionated assemblage. *American Journal of Science* **299**, 210–37.

Abdel-Rahman, A. M. & Martin, R. F. 1990. The Mount Gharib A-type granite, Nubian shield: petrogenesis and role of metasomatism at the source. *Contributions to Mineralogy and Petrology* **104**, 173–83.

Abdel-Rahman, A. M. & Nader, F. H. 2002. Characterization of the Lebanese Jurassic–Cretaceous carbonate stratigraphic sequence: A geochemical approach. *Geological Journal* **37**, 69–91.

Allègre, C. J., Hamelin, B., Provost, A. & Dupré, B. 1987. Topology in isotopic multispace and origin of mantle chemical heterogeneities. *Earth and Planetary Science Letters* **81**, 319–37.

Arkell, W. J. 1956. *Jurassic Geology of the World.* Edinburgh: Oliver and Boyd, 806 pp.

Baer, G., Heimann, A., Eshet, Y., Weinberger, R., Mussett, A. & Sherwood, G. 1995. The Saharonim basalt: A Late Triassic–Early Jurassic intrusion in southeastern Makhtesh Ramon, Israel. *Israel Journal of Earth Sciences* **44**, 1–10.

Baker, P. E. 1973. Islands in the South Atlantic. In *The Ocean Basins and Margins; Vol. 1, The South Atlantic* (eds A. E. H. Nairn and F. G. Stehli), pp. 493–553. New York: Plenum.

Barberi, F., Ferrara, G., Santacroce, R., Treuil, M. & Varet, J. 1975. A transitional basalt-pantellerite sequence of fractional crystallization: The Boina center (Afar rift, Ethiopia). *Journal of Petrology* **16**, 22–56.

Batiza, R. 1980. Origin and petrology of young oceanic central volcanoes: Are most tholeiitic rather than alkalic? *Geology* **8**, 477–82.

Ben-Avraham, Z. 1989. Multiple opening and closing of the eastern Mediterranean and south China basins. *Tectonics* **8**, 351–62.

Ben-Avraham, Z. & Ginzburg, A. 1990. Displaced terranes and crustal evolution of the Levant and eastern Mediterranean. *Tectonics* **9**, 613–22.

Ben Othman, D., Fourcade, S. & Allègre, C. J. 1984. Recycling processes in granite–granodiorite complex genesis: The Querigut case studied by Nd–Sr isotope systematics. *Earth and Planetary Science Letters* **69**, 290–300.

Bhat, M. L., Le Fort, P. & Ahmad, T. 1994. Bafliaz volcanics, NW Himalaya: Origin of a bimodal, tholeiitic, and alkali basalt suite. *Chemical Geology* **114**, 217–34.

Bizouard, H., Barberi, F. & Varet, J. 1980. Mineralogy and petrology of Erta Ale and Boina volcanic series, Afar rift, Ethiopia. *Journal of Petrology* **21**, 401–36.

Bradshaw, T. K. & Smith, E. I. 1994. Polygenetic Quaternary volcanism at Crater Flat, Nevada. *Journal of Volcanology and Geothermal Research* **63**, 165–82.

Chauvel, G., Hofmann, A. W. & Vidal, P. 1992. HIMU-EM, the French Polynesian connection. *Earth and Planetary Science Letters* **110**, 99–119.

Chen, W. & Arculus, R. J. 1995. Geochemical and isotopic characteristics of lower crustal xenoliths, San Francisco Volcanic Field, Arizona, U.S.A. *Lithos* **36**, 203–25.

Coulon, C., Vidal, P., Dupuy, C., Baudin, P., Popoff, M., Maluski, H. & Hermitte, D. 1996. The Mesozoic to Early Cenozoic magmatism of the Benue Trough (Nigeria); geochemical evidence for the involvement of the St Helena plume. *Journal of Petrology* **37**, 1341–58.

Dobosi, G. 1989. Clinopyroxene zoning patterns in the young alkali basalts of Hungary and their petrogenetic significance. *Contributions to Mineralogy and Petrology* **101**, 112–21.

Dvorkin, A. & Kohn, B. P. 1989. The Asher volcanics, northern Israel: Petrography, mineralogy and alteration. *Israel Journal of Earth Sciences* **38**, 105–23.

Dubertret, L. 1955. *Carte Geologique du Liban aux 1/200,000, avec notice explicative.* Ministire des Travaux Public, Beyrouth.

Dubertret, L. 1963. Liban, Syrie: Chaîne des grands massif côtiers et confins à I'Est. In *Lexique Stratigraphique International, 3, Asie* (ed. L. Dubertret), pp. 9–103. CNRS Paris: Fascicule 10 cl.

Dubertret, L. 1975. Introduction a la carte geologique a 1/150,000 du Liban. *Notes et Memoir Moyen Orient* **23**, 343–403.

Ellam, R. M. 1992. Lithospheric thickness as a control on basalt geochemistry. *Geology* **20**, 153–6.

Fitton, J. G., James, D. & Leeman, W. P. 1991. Basic magmatism associated with Late Cenozoic extension in the western United States: compositional variations in space and time. *Journal of Geophysical Research* **96**, 13693–712.

Francis, D. 1995. The implications of picritic lavas for the mantle source of terrestrial volcanism. *Lithos* **34**, 89–105.

Freund, R., Goldberg, M., Weissbrod, T., Druckman, Y. & Derin, B. 1975. The Triassic–Jurassic structure of Israel and its relation to the eastern Mediterranean. *Israel Geological Survey Bulletin* **65**, 26 pp.

Frey, F. A., Clague, D., Mahoney, J. J. & Sinton, J. M. 2000. Volcanism at the edge of the Hawaiian plume: petrogenesis of submarine alkalic lavas from the North Arch Volcanic Field. *Journal of Petrology* **41**, 667–91.

Frey, F. A., Garcia, M. O., Wise, W. S., Kennedy, A., Gurriet, P. & Albarede, F. 1991. The evolution of Mauna Kea volcano, Hawaii: Petrogenesis of tholeiitic and alkali basalts. *Journal of Geophysical Research* **96**, 14347–75.

Frey, F. A., Green, D. H., & Roy, S. D. 1978. Integrated models of basalt petrogenesis: a study of quartz tholeiites to olivine melilites from southeastern Australia utilizing geochemical and experimental data. *Journal of Petrology* **19**, 463–513.

Garfunkel, Z. 1981. Internal structure of the Dead Sea leaky transform (rift) in relation to plate kinematics. *Tectonophysics* **80**, 81–108.

Garfunkel, Z. 1989. Tectonic setting of Phanerozoic magmatism in Israel. *Israel Journal of Earth Sciences* **38**, 51–74.

Garfunkel, Z. 1992. Darfur-Levant array of volcanics – a 140-Ma-long record of a hotspot beneath the African–Arabian continent, and its bearing on Africa's absolute motion. *Israel Journal of Earth Sciences* **40**, 135–50.

Garfunkel, Z. 1998. Constraints on the origin and history of the Eastern Mediterranean basin. *Tectonophysics* **298**, 5–35.

Gibson, S. A., Thompson, R. N., Weska, R. K., Dickin, A. P. & Leonardos, O. H. 1997. Late Cretaceous rift-related upwelling and melting of the Trinidad starting mantle plume head beneath western Brazil. *Contributions to Mineralogy and Petrology* **126**, 303–14.

Ginzburg, A. & Ben-Avraham, Z. 1987. The deep structure of the central and southern Levant continental margin. *Annals Tectonicae* **1**, 105–15.

Gvirtzman, Z., Garfunkel, Z. & Rotstein, Y. 1994. Mesozoic magmatism in the central Negev (southern Israel): Implications from magnetic anomalies. *Israel Journal of Earth Sciences* **43**, 21–38.

Gvirtzman, Z., Klang, A. & Rotstein, Y. 1992. Early Jurassic shield volcano below Mount Carmel: New interpratation of the magnetic and gravity anomalies and implication for Early Jurassic rifting. *Israel Journal of Earth Sciences* **39**, 149–59.

Gvirtzman, Z., Weissbrod, T., Baer, G. & Brenner, G. J. 1996. The age of the Aptian stage and its magnetic events: new Ar–Ar ages and palaeomagnetic data from the Negev, Israel. *Cretaceous Research* **17**, 293–310.

Haase, K. M. 1996. The relationship between the age of the lithosphere and the composition of oceanic magmas: constraints on partial melting, mantle sources, and the thermal structure of the plates. *Earth and Planetary Science Letters* **144**, 75–92.

Haase, K. M. & Devey, C. D. 1994. The petrology and geochemistry of Vesteris Seamount, Greenland Basin–an intraplate alkaline volcano of non-plume origin. *Journal of Petrology* **35**, 295–328.

Haase, K. M., Stoffers, P. & Garbe-Schönberg, C. D.

1997. The petrogenetic evolution of lavas from Easter Island and neighbouring seamounts, Near-ridge hotspot volcanoes in SE Pacific. *Journal of Petrology* **38**, 785–813.

Halliday, A. N., Davidson, J. P., Holden, P., DeWolf, C., Lee, D.-C. & Fitton, J. G. 1990. Trace-element fractionation in plumes and the origin of HIMU mantle beneath the Cameroon line. *Nature* **347**, 523–8.

Halliday, A. N., Dickin, A. P., Fallick, A. E. & Fitton, J. G. 1988. Mantle dynamics: a Nd, Sr, Pb and O isotopic study of the Cameroon Line volcanic chain. *Journal of Petrology* **29**, 181–211.

Hanson, G. N. 1980. Rare earth elements in petrogenetic studies of igneous systems. *Annual Reviews in Earth Sciences* **8**, 371–406.

Hart, S. R. 1988. Heterogeneous mantle domains signatures, genesis and mixing chronologies. *Earth and Planetary Science Letters* **90**, 273–96.

Hart, W. K., Wolde, G. C., Walter, R. C. & Mertzman, S. A. 1989. Basaltic volcanism in Ethiopia: constraints on continental rifting and mantle interactions. *Journal of Geophysical Research* **94**, 7731–48.

Hirsch, F., Flexer, A., Rosenfeld, A. & Yellin-Dror, A. 1995. Palinspatic and crustal setting of the eastern Mediterranean. *Journal of Petroleum Geology* **18**, 149–70.

Hoernle, K. & Schmincke, H. U. 1993. The role of partial melting in the 15 Ma geochemical erosion of Gran Canaria: a blob model for the Canary hotspot. *Journal of Petrology* **34**, 599–626.

Hofmann, A. W. 1997. Mantle geochemistry: the message from oceanic volcanism. *Nature* **385**, 219–29.

Khair, K. & Tsokas, G. N. 1999. Nature of the Levantine (eastern Mediterranean) crust from multiple-source Werner deconvolution of Bouguer gravity anomalies. *Journal of Geophysical Research* **104**, 25469–78.

Knipper, A. L. & Sharaskin, A. Y. 1994. Tectonic evolution of the western part of the Peri-Arabian ophiolite arc. In *Geological Structures of the northeastern Mediterranean (Cruise 5 of the Research Vessel 'Akademik Nikolaj Strakhov')* (eds V. A. Krasheninnikov and J. K. Hall), pp. 295–305. Jerusalem: Hist. Productions – Hall.

Kohn, B. P., Lang, B. & Steinitz, G. 1993. $^{40}Ar/^{39}Ar$ dating of the atlit-1 volcanic sequence, northern Israel. *Israel Journal of Earth Sciences* **42**, 17–28.

Lang, B., Hebeda, E. H., Priem, H. N. A., Steinitz, G. & Verdurmen, E. A. Th. 1988. K–Ar and Rb–Sr ages of Early Cretaceous magmatic rocks from Makhtesh Ramon, southern Israel. *Israel Journal of Earth Sciences* **37**, 65–72.

Lang, B. & Steinitz, G. 1987. K–Ar dating of subsurface Mesozoic and Cenozoic magmatic rocks in Israel. *Geological Survey of Israel Report* **GSI/8/87**, 48 pp.

Lang, B. & Steinitz, G. 1989. K–Ar dating of Mesozoic magmatic rocks in Israel. *Israel Journal of Earth Sciences* **38**, 89–104.

Lassiter, J. C., DePaolo, D. J. & Mahoney, J. J. 1995. Geochemistry of the Wrangellia Flood Basalt Province: implications for the role of continental and oceanic lithosphere in flood basalt genesis. *Journal of Petrology* **36**, 983–1009.

Laws, E. D. & Wilson, M. 1997. Tectonics and magmatism associated with Mesozoic passive continental margin development in the Middle East. *Journal of the Geological Society, London* **154**, 757–60.

Le Bas, M. J., Le Maitre, R. W., Streckeisen, A. L. & Zanettin, B. 1986. A chemical classification of volcanic rocks based on the total alkali-silica diagram. *Journal of Petrology* **27**, 745–50.

Le Bas, M. J. & Streckeisen, A. L. 1991. The IUGS systematics of igneous rocks. *Journal of the Geological Society of London* **148**, 825–33.

Lee, D. C., Halliday, A. N., Fitton, J. G. & Poli, G. 1994. Isotopic variation with distance and time in the volcanic islands of the Cameroon Line: evidence for a mantle plume origin. *Earth and Planetary Science Letters* **123**, 119–38.

Longerich, H. P., Jenner, G. A., Fryer, B. J. & Jackson, S. E. 1990. Inductively coupled plasma – mass spectrometric analysis of geological samples: A critical evaluation based on case studies. *Chemical Geology* **83**, 105–18.

Maaløe, S. & Aoki, K. 1977. The major element composition of the upper mantle estimated from the composition of lherzolites. *Contributions to Mineralogy and Petrology* **63**, 161–73.

Maluski, H., Coulon, C., Popoff, M., & Baudin, P. 1995. $^{40}Ar/^{39}Ar$ chronology, petrology and geodynamic setting of Mesozoic to early Cenozoic magmatism from the Benue Trough, Nigeria. *Journal of the Geological Society, London* **152**, 311–26.

McKenzie, D. P. & O'Nions, R. K. 1991. Partial melting distributions from inversion of rare earth element concentrations. *Journal of Petrology* **32**, 1021–91.

Melluso, L., Beccaluva, L., Brotzu, P., Gregnanin, A., Gupta, A. K., Morbidelli, L. & Traversa, G. 1995. Constraints on the mantle sources of the Deccan Traps from the petrology and geochemistry of the basalts of Gujarat State (Western India). *Journal of Petrology* **36**, 1393–432.

Menzies, M. A. & Kyle, R. 1990. Continental volcanism: a crust-mantle probe. In *Continental Mantle* (ed. M. A. Menzies), pp. 157–77. Oxford: Oxford Science Publishers.

Mouty, M., Delaloye, M., Fontignie, D., Piskin, O. & Wagner, J.-J. 1992. The volcanic activity in Syria and Lebanon between Jurassic and actual. *Schweizerische Mineralogische und Petrografische Mitteilungen* **72**, 91–105.

Nicholson, H. & Latin, D. 1992. Olivine tholeiites from Krafla, Iceland: evidence for variation in melt fraction within a plume. *Journal of Petrology* **33**, 1105–24.

Pankhurst, R. J. 1977. Open system fractionation and incompatible element variations in basalts. *Nature* **268**, 36–8.

Pearce, J. A. & Norry, M. J. 1979. Petrogenetic implications of Ti, Zr, Y, and Nb variations in volcanic rocks. *Contributions to Mineralogy and Petrology* **69**, 33–47.

Raad, K. 1979. *Les Formations Volcaniques du Liban*. Docteur 3e cycle, Université de Paris-Sud, Centre d'Orsay, France, 114 pp.

Renouard, G. 1951. Sur la Découverte du Jurassique Inférieur et du Jurassique Moyen du Liban. *Centre de Recherche Academie Scientifique, Paris, France* **232**, 992–4.

Richard, P., Shimizu, N. & Allègre, C. J. 1976. $^{143}Nd/^{144}Nd$, a natural tracer: an application to oceanic basalts. *Earth and Planetary Science Letters* **31**, 269–78.

Robertson, A. H. F., Clift, P. D., Degnan, P. J. & Jones, G. 1991. Palaeogeographic and palaeotectonic evolution of the eastern Mediterranean Neotethys. *Palaeogeography, Palaeoclimatology, Palaeoecology* **87**, 289–343.

Shaw, D. M. 1970. Trace element fractionation during anatexis. *Geochimica et Cosmochimica Acta* **34**, 237–43.

Shervais, J. W. 1982. Ti–V plots and the petrogenesis of modern ophiolite lavas. *Earth and Planetary Science Letters* **59**, 101–18.

Shimron, A. E. & Lang, B. 1989. Cretaceous magmatism along the southern flank of Mount Hermon. *Israel Journal of Earth Sciences* **38**, 125–42.

Smith, E.I., Sánchez, A., Walker, J. D. & Wang, K. 1999. Geochemistry of mafic magmas in the Hurricane Volcanic Field, Utah: implications for small- and large-scale chemical variability of the lithospheric mantle. *Journal of Geology* **107**, 433–48.

Späth, A., Le Roex, A. P. & Duncan, R. A. 1996. The geochemistry of lavas from the Comores Archipelago, Western Indian Ocean: petrogenesis and mantle source region characteristics. *Journal of Petrology* **37**, 961–91.

Staudigel, H., Zindler, A., Hart, S. R., Leslie, C. Y. & Clague, D. 1984. The isotope systematics of a juvenile intra-plate volcano: Pb, Nd and Sr isotope ratios of basalts from Loihi Seamount, Hawaii. *Earth and Planetary Science Letters* **69**, 13–29.

Sun, S. & McDonough, W. F. 1989. Chemical and isotopic systematics of oceanic basalts: implications for mantle composition and processes. In *Magmatism in the ocean basins* (eds A. D. Saunders and M. J. Norry), pp. 313–45. Geological Society of London, Special Publication no. 42.

Thompson, R. N., Morrison, M. A., Hendry, G. L. & Parry, S. J. 1984. An assessment of the relative roles of crust and mantle in magma genesis: an element approach. *Royal Society Philosophical Transactions, London* **A310**, 549–90.

Wallace, P. & Carmichael, I. S. E. 1992. Alkaline and calc-alkaline lavas near Los Volcanes, Jalisco, Mexico: geochemical diversity and its significance in volcanic arcs. *Contributions to Mineralogy and Petrology* **111**, 423–39.

Walley, C. D. 1997. The Lithostratigraphy of Lebanon. *Lebanese Science Bulletin* **10**, 81–108.

Weaver, B. L. 1991. Trace element evidence for the origin of ocean-island basalts. *Geology* **19**, 123–6.

Weaver, B. L., Wood, D. A., Tarney, J. & Joron J. 1987. Geochemistry of ocean ialand basalts from the South Atlantic: Ascension, Bouvet, St. Helena, Gough and Tristan da Cunda. In *Alkaline Igneous Rocks* (eds J. G. Fitton and B. G. J. Upton), pp. 253–67. Geological Society of London, Special Publication no. 30.

White, W. M. 1985. Sources of oceanic basalts: radiogenic isotopic evidence. *Geology* **13**, 115–18.

White, R. & McKenzie, D. 1989. Magmatism at rift zones: the generation of volcanic continental margins and flood basalts. *Journal of Geophysical Research* **94**, 7685–729.

Wilson, M. 1993. Geochemical signatures of oceanic and continental basalts: a key to mantle dynamics? *Journal of the Geological Society, London* **150**, 977–90.

Winchester, J. A. & Floyd, P. A. 1977. Geochemical discrimination of different magma series and their differentiation products using immobile elements. *Chemical Geology* **20**, 325–43.

Witt-Eickschen, G. & Kramm, U. 1997. Mantle upwelling and metasomatism beneath central Europe: geochemical and isotopic constraints from mantle xenoliths from the Rhon (Germany). *Journal of Petrology* **38**, 479–93.

Wittke, J. H. & Mack, L.E. 1993. OIB-like mantle source for continental alkaline rocks of the Balcones province, Texas: trace element and isotopic evidence. *Journal of Geology* **101**, 333–44.

Zindler, A. & Hart, S. R. 1986. Chemical geodynamics. *Annual Reviews of Earth and Planetary Sciences* **14**, 493–571.